
Article:
Zubi, A., Alnafisah, H.A., Turega, S. et al. (4 more authors) (2022) Being positive is not everything – experimental and computational studies on the selectivity of a self-assembled, multiple redox-state receptor that binds anions with up to picomolar affinities. Chemistry – A European Journal, 28 (5). e202102465. ISSN 0947-6539

https://doi.org/10.1002/chem.202102465

Being positive is not everything – experimental and computational studies on the selectivity of a self-assembled, multiple redox-state, receptor that binds anions with up to picomolar affinities

Ahmed Zubi,[‡a] Hawazin A Alnafisah,[a,b] Simon Turega,[c] Igor Marques,[d] José R. B. Gomes,[d] Jim A. Thomas,[a]* and Vítor Félix[d]*

[a] Department of Chemistry, University of Sheffield, Brook Hill, Sheffield, S3 7HF, UK

[b] Department of Chemistry, Princess Nourah Bint Abdulrahman University, Riyadh, Saudi Arabia

[c] Department of Bioscience and Chemistry, Sheffield Hallam University, Howard Street, Sheffield, S1 1WB, UK

[d] CICECO – Aveiro Institute of Materials, Department of Chemistry, University of Aveiro, 3810-193, Aveiro, Portugal

[‡] Current address: Chemistry Department, Faculty of Science Misurata University, Misurata, Libya

NMR Titrations

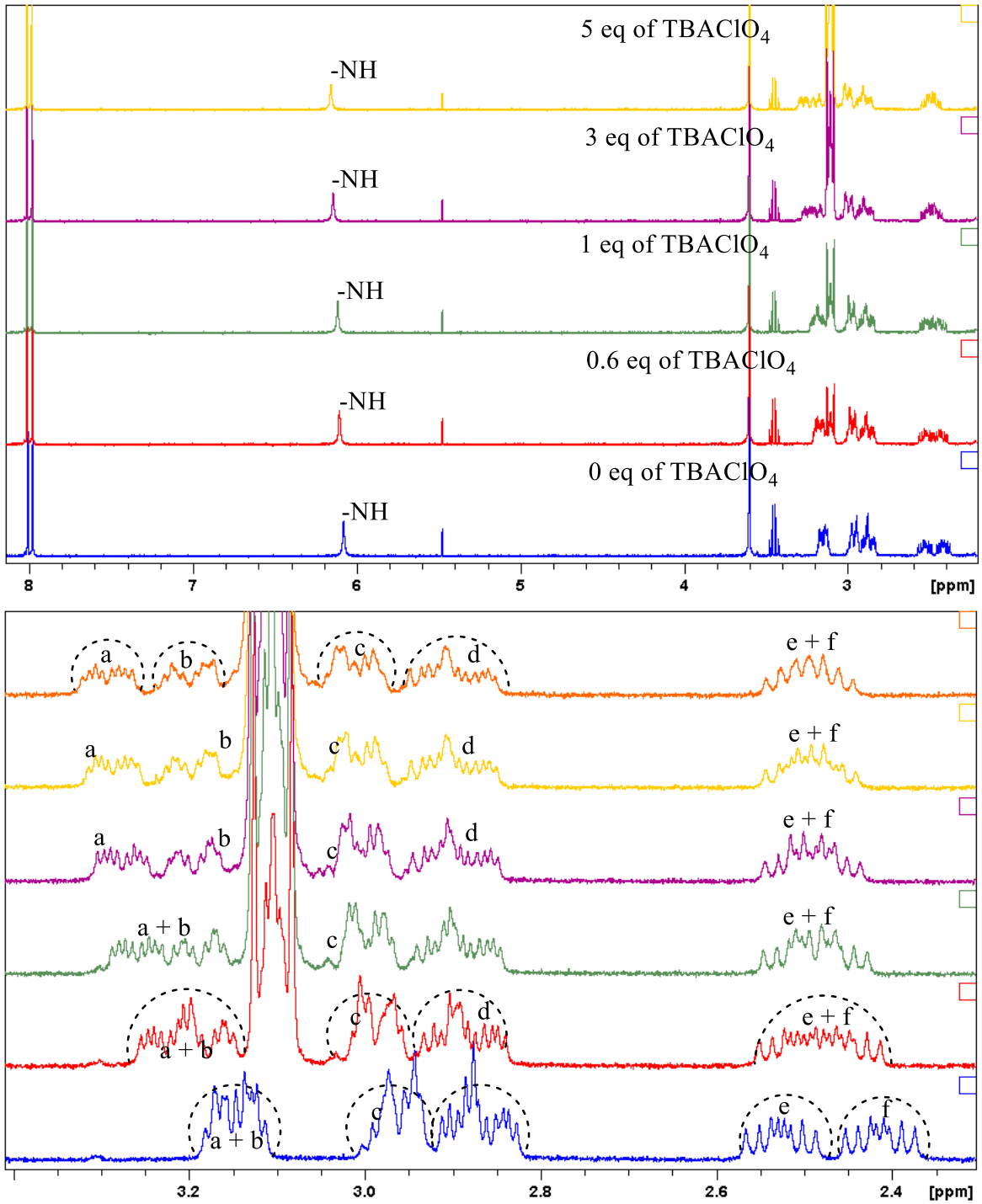

Fig. S1. Details of ^{1}H NMR (400 MHz) spectra of $\mathbf{1}^{3+}$ upon addition of equivalents of $TBAClO_4$. Solvent CD_3CN; temperature: 293 K; [$\mathbf{1}^{3+}$] =1.5×10^{-6} mol dm^{-3}. Top: Shifts in N–H signals of 9MA bridging ligand. Bottom: Thiacrown region.

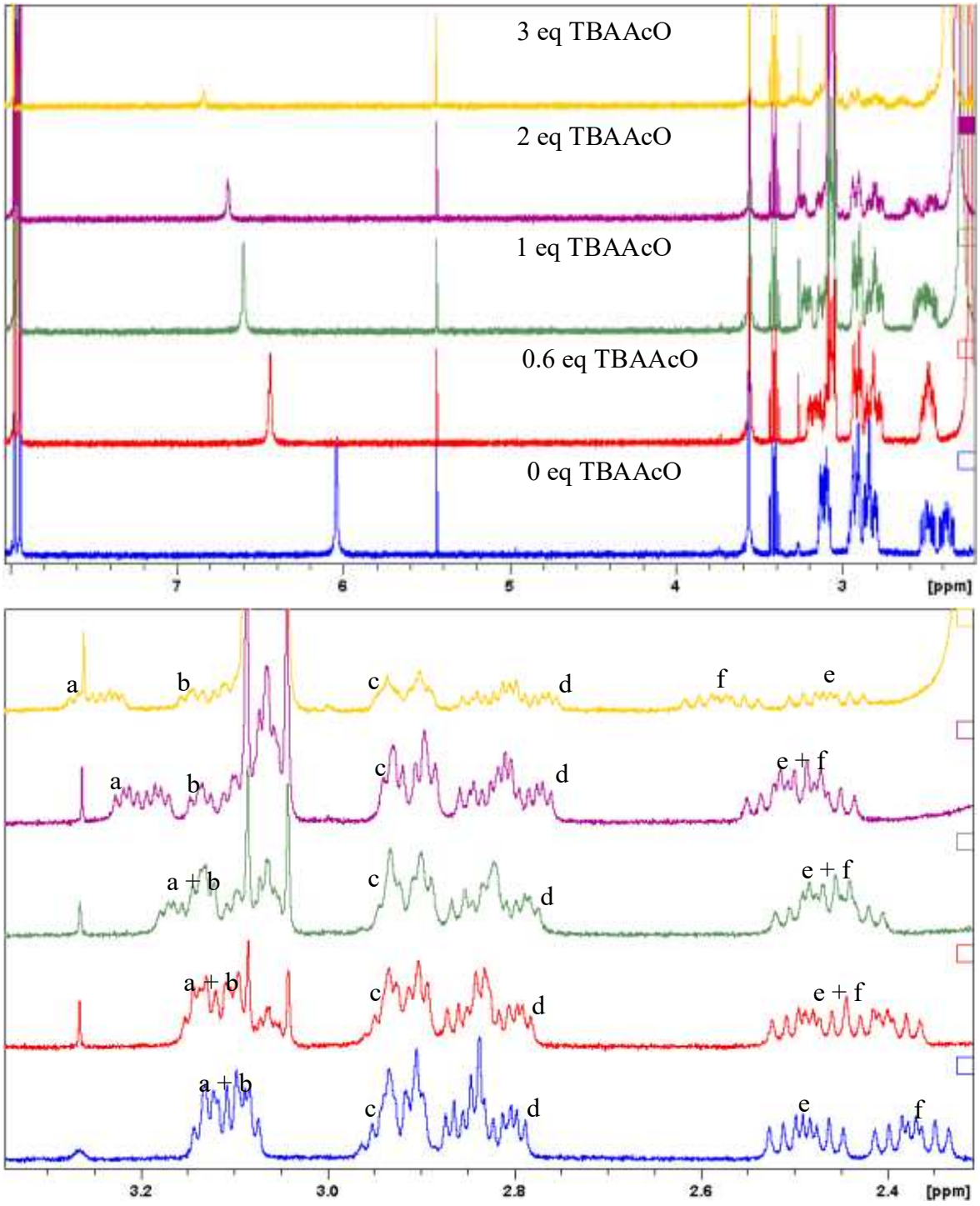

Fig. S2. Details of ^{1}H NMR (400 MHz) spectra of $\mathbf{1}^{3+}$ upon addition of equivalents of TBAAcO. Solvent CD_3CN; temperature: 293 K; [$\mathbf{1}^{3+}$] =1.5×10^{-6} mol dm^{-3}. Top: Shifts in N–H signals of 9MA bridging ligand. Bottom: Thiacrown region.

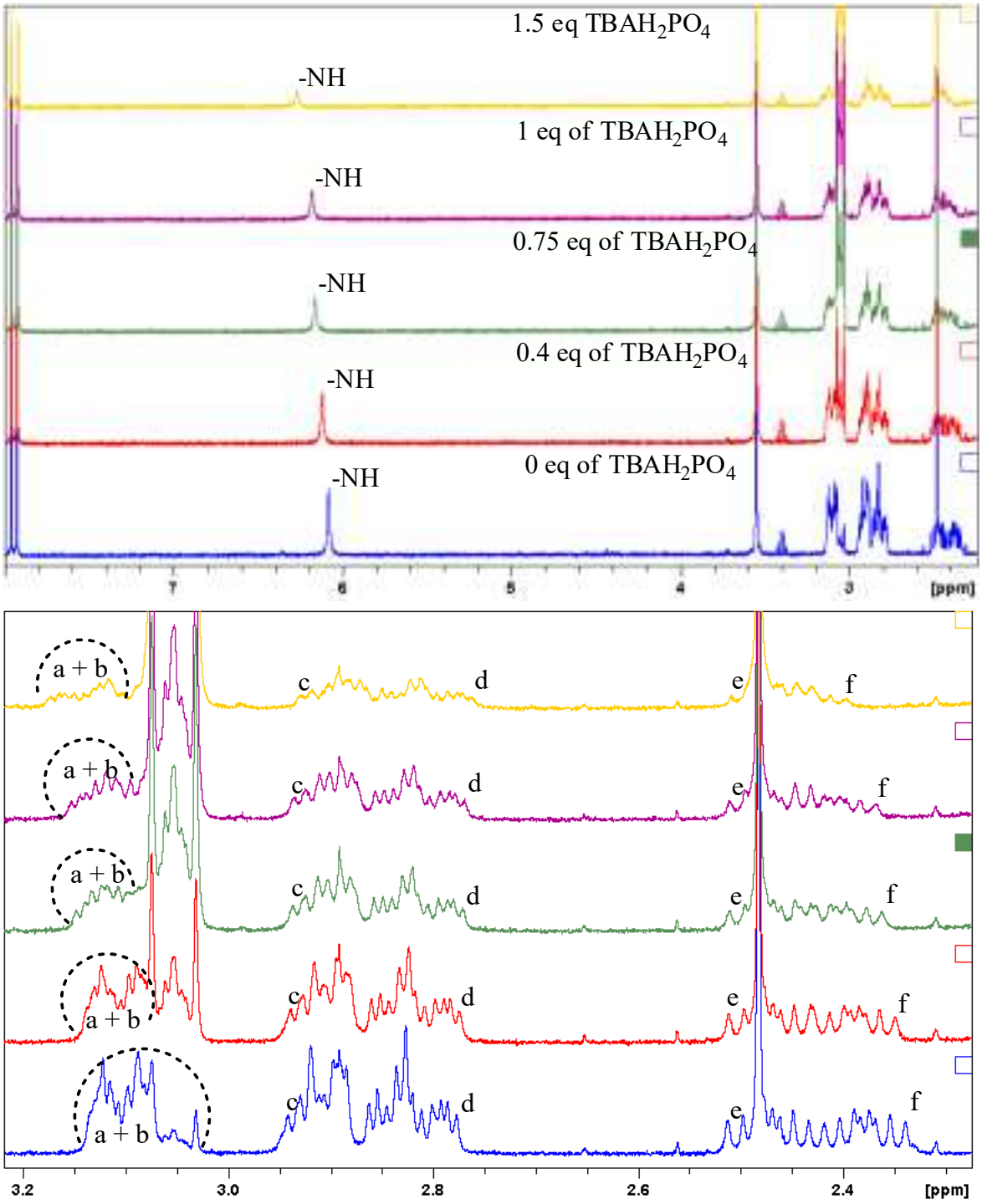

Fig. S3. Details of ^{1}H NMR (400 MHz) spectra of $\mathbf{1}^{3+}$ upon addition of equivalents of $TBAH_2PO_4$. Solvent CD_3CN; temperature: 293 K; [$\mathbf{1}^{3+}$] =1.5×10^{-6} mol dm^{-3}. Top: Shifts in N–H signals of 9MA bridging ligand. Bottom: Thiacrown region.

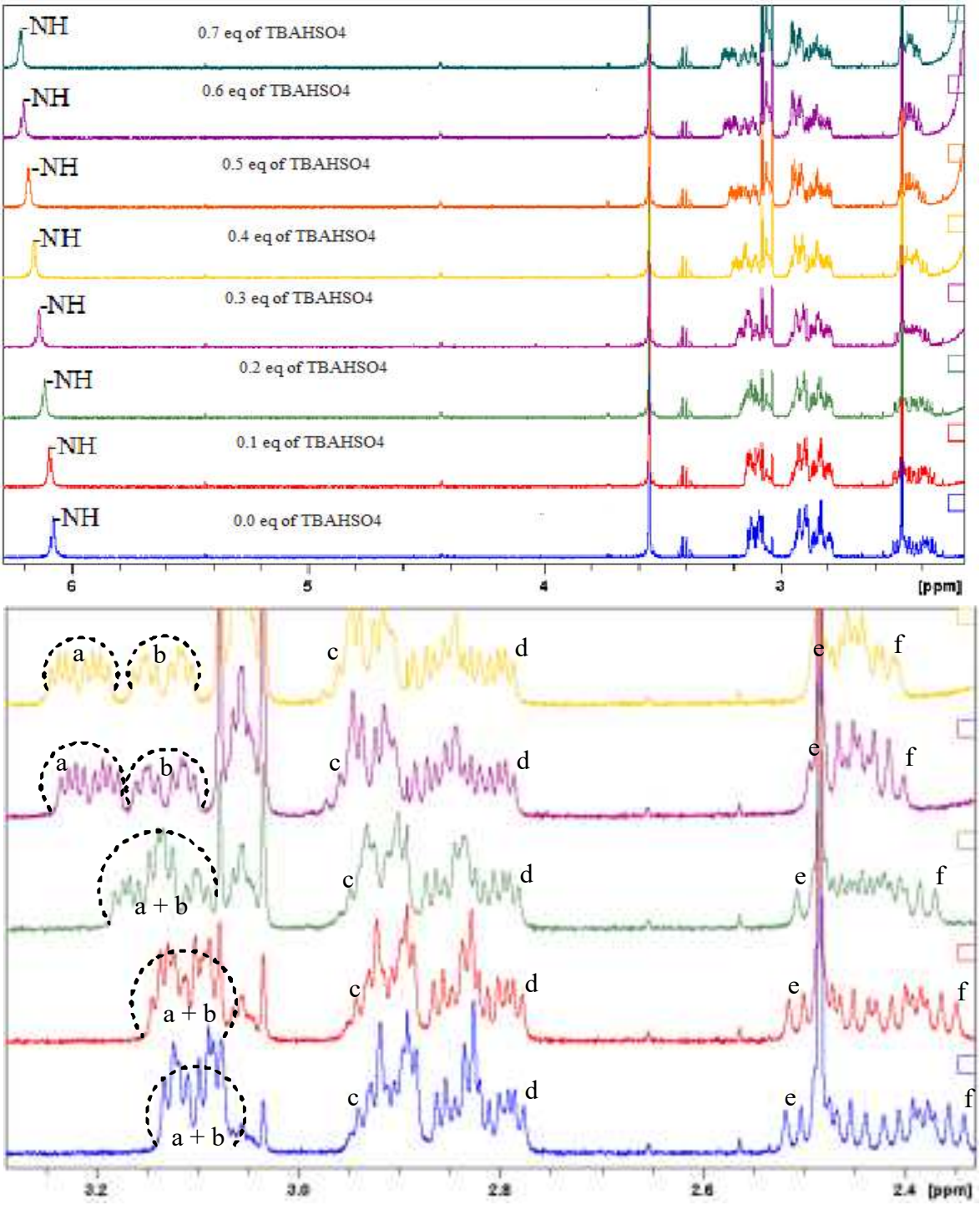

Fig. S4. Details of ^{1}H NMR (400 MHz) spectra of $\mathbf{1}^{3+}$ upon addition of equivalents of $TBAHSO_4$. Solvent CD_3CN; temperature: 293 K; $[\mathbf{1}^{3+}] = 1.5\times10^{-6}$ mol dm^{-3}. Top: Shifts in N–H signals of 9MA bridging ligand. Bottom: Thiacrown region.

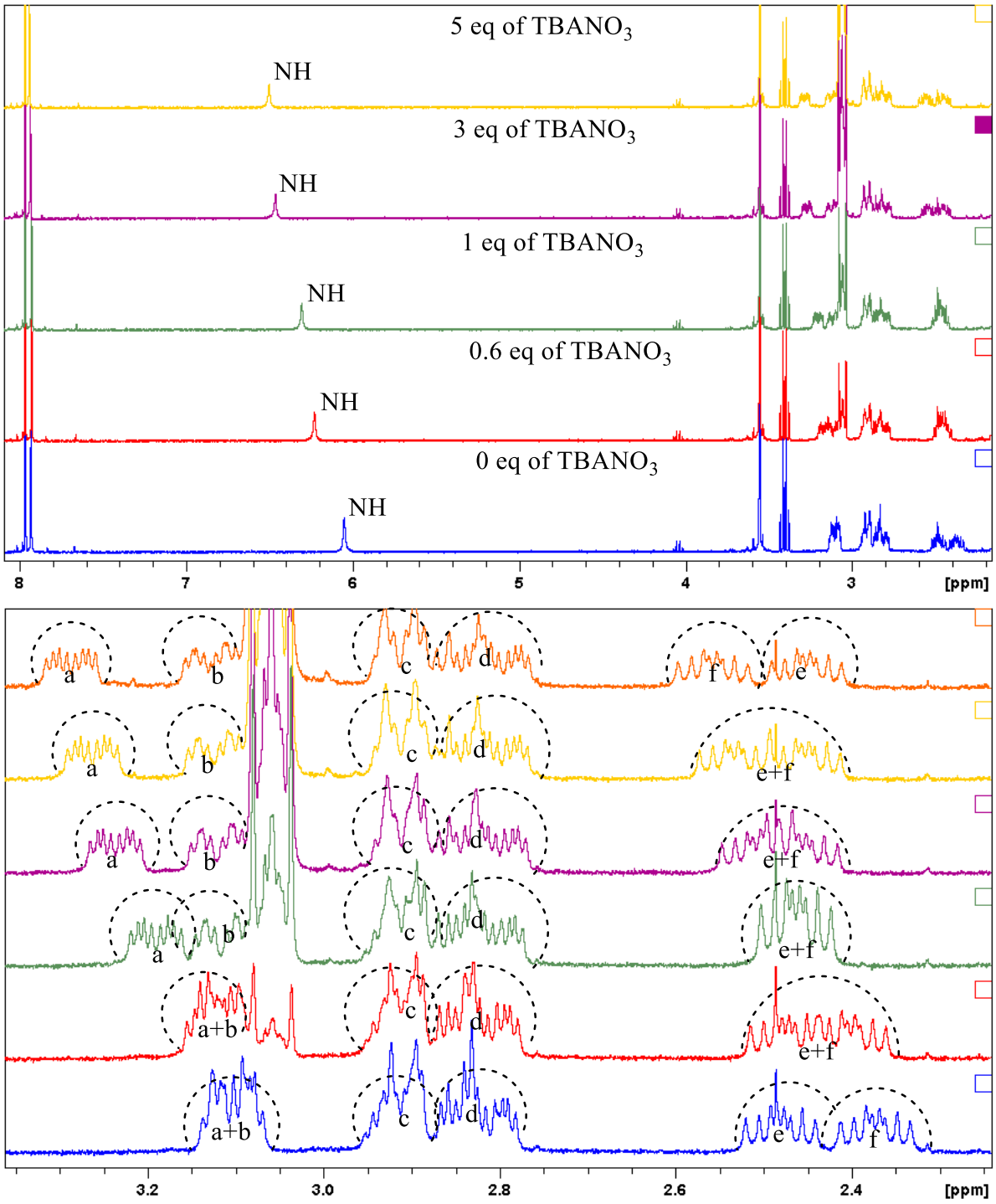

Fig. S5. Details of ^{1}H NMR (400 MHz) spectra of $\mathbf{1}^{3+}$ upon addition of equivalents of $TBANO_3$. Solvent CD_3CN; temperature: 293 K; $[\mathbf{1}^{3+}] = 1.5\times10^{-6}$ mol dm^{-3}. Top: Shifts in N–H signals of 9MA bridging ligand. Bottom: Thiacrown region.

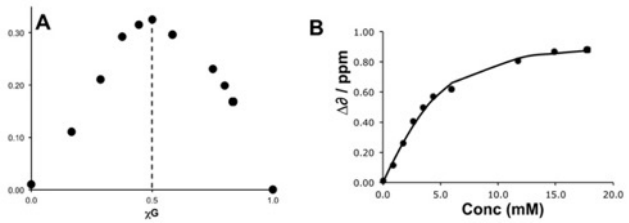

Fig. S6. A – Example of ^{1}H-NMR-based Job plot for the interaction of $\mathbf{1}^{3+}$ with acetate in d_3-MeCN; **B** – ^{1}H-NMR-based titration with the same anion using shifts in N–H protons of the 9MA. The continuous line is a fit to a 1:1 binding isotherm.

Electrochemical Data

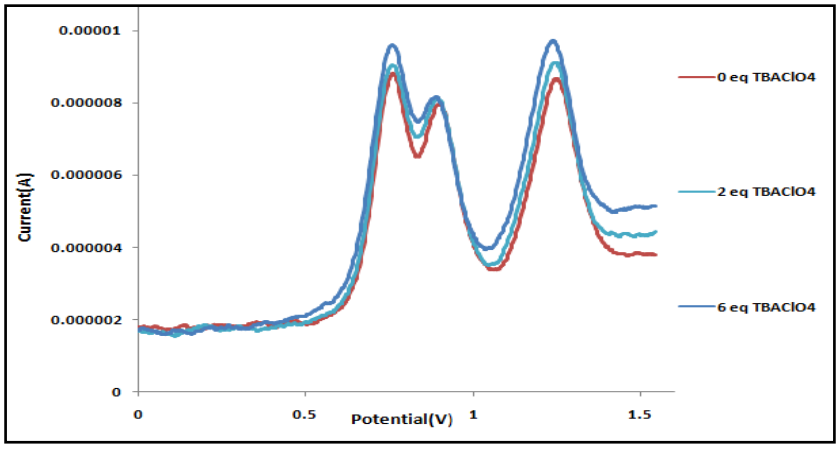

Fig. S7. SWV of macrocycle $\mathbf{1}^{3+}$ upon the addition of aliquots of perchlorate anion.

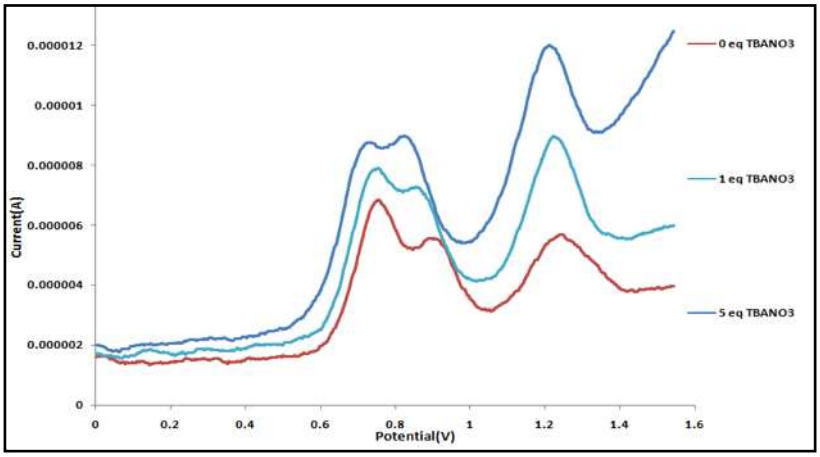

Fig. S8. SWV of macrocycle $\mathbf{1}^{3+}$ upon the addition of aliquots of nitrate anion.

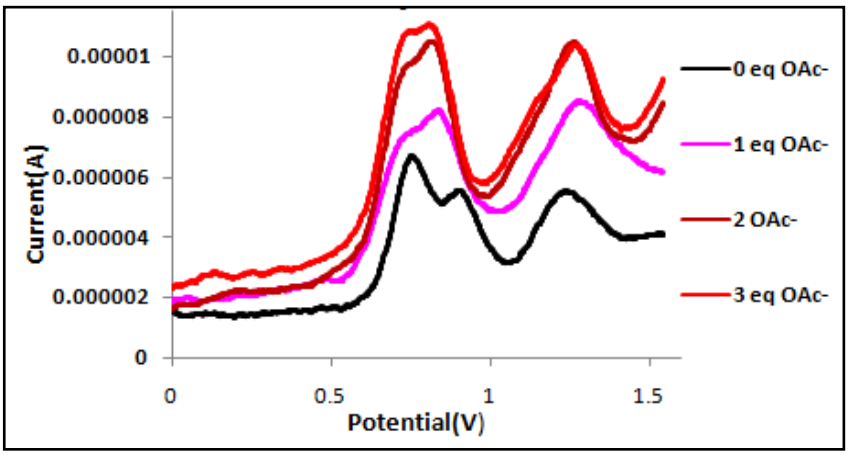

Fig. S9. SWV of macrocycle $\mathbf{1}^{3+}$ upon the addition of aliquots of acetate anion.

Table S1. Maximum electrochemical shifts (mV) for [**1**]$(PF_6)_3$ induced by addition of oxo anions.[a]

Anion	ΔEp(1)	ΔEp(2)	ΔEp(3)
ClO_4^-	–10	–10	–35
NO_3^-	–50	–70	–45
CH_3COO^-	–15	–115	0

[a] In these conditions, the three oxidations of [**1**]$(PF_6)_3$ on its own were observed at 0.775 V, 0.910 V, and 1.270 V, respectively.

Crystallographic Studies

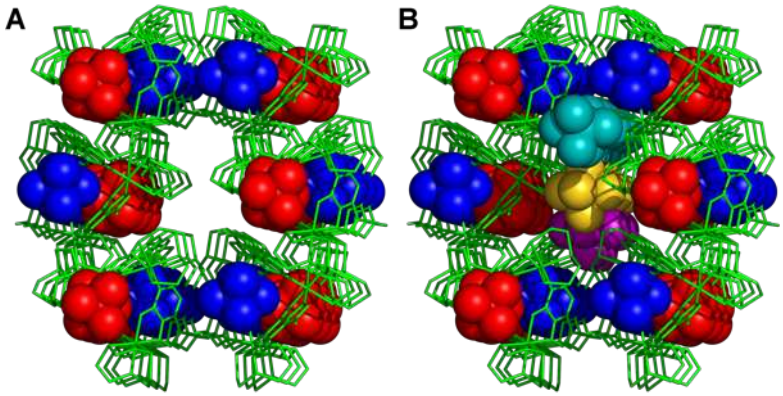

Fig. S10. **A** – Hexagonal channels defined by the interaction between the host and anions; **B** – Hexagonal channels filled with the remaining hexafluorophosphate anions.

Computational Studies

Detailed Methods

All DFT calculations were carried out with Gaussian09,[1] using the CAM-B3LYP[2] functional with Grimme's D3 dispersion correction[3] and a polarised continuous solvent model (IEFPCM)[4] for MeCN. Tight SCF convergence criterium was used, together with an ultrafine grid for numerical integrations. The ruthenium centres were described with the LANL2TZ(f) basis set,[5] while the 6-31+G(d) basis set was used for the remaining elements. The stability of the wavefunction in all DFT optimised structures was assessed by the use of the Gaussian keyword "stable=opt". In the initial DFT optimisation of the *ls*-$\mathbf{1}^{5+}$ systems, the wavefunction revealed to be instable. These systems were re-optimised with the newly calculated wavefunction as guess. Finally, each DFT optimised structure was ascertained to be a minimum, as no imaginary frequencies were found.

The electrostatic potential distributions of free $\mathbf{1}^{n+}$ were mapped onto their electron density surfaces (V_S, estimated at 0.001 $e a_0^{-3}$) with MultiWFN 3.6[6] along the four oxidation states. The V_S of all anions was determined following the same approach, leading to their $V_{S,min}$ values and molecular volumes (see main text). The interactions

between $\mathbf{1}^{n+}$ and the anion guests were evaluated through the Quantum Theory of Atoms in Molecules (QTAIM)[7] as implemented in MultiWFN 3.6,[6a] as well as by the Natural Bond Orbital (NBO) analysis,[8] using NBO 6.0.[9]

The binding enthalpy (ΔH_{HG}) for the host-guest associations between $\mathbf{1}^{n+}$ and the anions was estimated through the following equation:

$$\Delta H_{HG} = H_{HG} - H_H - H_G \qquad \text{Eq. S1}$$

where H_{HG}, H_H and H_G correspond to the enthalpies estimated from the DFT IEFPCM ground state optimised structures of the host-guest association (HG), the macrocyclic host (H), and the oxo-anion guest (G), respectively. Each individual enthalpy term was obtained as $H = \mathcal{E}_0 + E_{tot} + RT$, where $\mathcal{E}_0$ is the total electronic energy, E_{tot} is the total internal energy, accounting the contributions from the translational, rotational, vibrational and electronic motions, while RT is the thermal correction, R being the constant for ideal gases and T the temperature. Furthermore, E_{tot} already includes the zero-point vibrational energy correction. Negative ΔH_{HG} values indicate that the formation of the host-guest association is favourable.

Supplementary Tables

Table S2. Comparison between the average Ru-S and Ru-N distances (Å) in the X-ray crystal structure of $\mathbf{1}^{3+}\cdot PF_6^-$ and in the DFT optimised structures of free $\mathbf{1}^{n+}$.

Distance	$\mathbf{1}^{3+}\cdot PF_6^-$	$\mathbf{1}^{3+}$	$\mathbf{1}^{4+}$	*ls*-$\mathbf{1}^{5+}$	*hs*-$\mathbf{1}^{5+}$	*ls*-$\mathbf{1}^{6+}$	*hs*-$\mathbf{1}^{6+}$
Ru–S	2.293 ± 0.006	2.360 ± 0.006	2.375 ± 0.025	2.388 ± 0.027	2.388 ± 0.026	2.398 ± 0.019	2.398 ± 0.019
Ru–N	2.159 ± 0.014	2.152 ± 0.007	2.131 ± 0.047	2.115 ± 0.057	2.115 ± 0.057	2.103 ± 0.060	2.105 ± 0.061

Table S3. Energy differences (kcal mol^{-1})[a,b] between the high- and low-spin electron configurations of free and anion associated $\mathbf{1}^{5+}$ and $\mathbf{1}^{6+}$, calculated using the DFT optimised structures.[c]

		Host	
Binding pocket	Guest anion	$\mathbf{1}^{5+}$	$\mathbf{1}^{6+}$
--	--	0.004	0.835
α	CH_3COO^-	0.066	1.007
	NO_3^-	0.075	1.076
	ClO_4^-	0.011	1.078
	HSO_4^-	-0.293	0.958
	$H_2PO_4^-$	0.028	1.041
	F^-	0.065	1.160
	Cl^-	0.094	1.114
	Br^-	0.181	1.052
	I^-	-0.115	0.989
	PF_6^-	0.143	0.895
β	CH_3COO^-[d]	0.158	0.840
	CH_3COO^-[e]	0.564	1.379
	NO_3^-	0.277	0.841
	ClO_4^-	-0.217	1.096
	HSO_4^-	0.025	0.905
	$H_2PO_4^-$	0.036	0.777
	F^-	1.007	1.130
	Cl^-	-0.124	0.855
	Br^-	0.181	0.862
	I^-	0.088	0.860
	PF_6^-	0.040	0.933

[a] Electronic energies, corrected with the zero-point vibrational energies; [b] the energy values were not corrected for basis set superposition errors; [c] positive values mean that the low-spin electron configuration is more favourable; [d] the methyl group is pointing inwards the binding pocket; and [e] the carboxylate group is pointing inwards the binding pocket.

Table S4. Electrostatic potential maxima assessed in the electron density surface of the α and β pockets of $\mathbf{1}^{n+}$ (kcal mol^{-1}).

Binding	Host					
pocket	$\mathbf{1}^{3+}$	$\mathbf{1}^{4+}$	*ls*-$\mathbf{1}^{5+}$	*hs*-$\mathbf{1}^{5+}$	*ls*-$\mathbf{1}^{6+}$	*hs*-$\mathbf{1}^{6+}$
α	204.101	276.914	348.970	345.491	417.143	412.115
β	134.175[a]	213.180	290.615	284.309	359.785	352.083[a]
$\Delta_{\alpha\text{-}\beta}$	69.926	63.734	58.355	61.182	57.357	60.032

[a] These species display three distinguishable V_S points with comparable values, which were averaged and have standard deviations of 0.073 and 0.137 kcal mol^{-1} for $\mathbf{1}^{3+}$ and *hs*-$\mathbf{1}^{6+}$, respectively.

Table S5. Mulliken spin densities (a.u.) on Ru centres in anion associations of $\mathbf{1}^{n+}$ (n = 4, 5 or 6).

Binding pocket	Guest anion	Host				
		$\mathbf{1}^{4+}$	*ls*-$\mathbf{1}^{5+}$	*hs*-$\mathbf{1}^{5+}$	*ls*-$\mathbf{1}^{6+}$	*hs*-$\mathbf{1}^{6+}$
α	CH_3COO^-	0.001 ; 0.687 ; 0.002	-0.670 ; -0.002 ; 0.784	0.645 ; 0.015 ; 0.779	0.775 ; -0.765 ; 0.795	0.796 ; 0.769 ; 0.789
	NO_3^-	0.719 ; 0.001 ; 0.001	0.681 ; 0.002 ; -0.781	0.656 ; 0.013 ; 0.773	0.810 ; 0.767 ; -0.779	0.806 ; 0.786 ; 0.786
	ClO_4^-	0.002 ; 0.708 ; 0.001	-0.676 ; -0.001 ; 0.795	0.652 ; 0.012 ; 0.788	0.784 ; -0.796 ; 0.806	0.803 ; 0.803 ; 0.803
	HSO_4^-	0.002 ; 0.705 ; 0.002	-0.800 ; 0.669 ; 0.002	0.656 ; 0.012 ; 0.790	0.787 ; -0.793 ; 0.804	0.807 ; 0.800 ; 0.800
	$H_2PO_4^-$	0.001 ; 0.002 ; 0.712	0.672 ; 0.002 ; -0.796	0.648 ; 0.013 ; 0.790	0.781 ; -0.788 ; 0.806	0.801 ; 0.794 ; 0.802
	F^-	0.679 ; 0.002 ; 0.000	0.768 ; -0.641 ; -0.003	0.615 ; 0.014 ; 0.759	-0.760 ; 0.769 ; 0.746	0.765 ; 0.764 ; 0.767
	Cl^-	0.706 ; 0.003 ; 0.001	-0.793 ; 0.670 ; 0.003	0.648 ; 0.015 ; 0.782	-0.795 ; 0.802 ; 0.784	0.804 ; 0.801 ; 0.805
	Br^-	0.710 ; 0.002 ; 0.001	0.796 ; -0.674 ; -0.002	0.654 ; 0.014 ; 0.786	0.809 ; 0.783 ; -0.798	0.807 ; 0.804 ; 0.807
	I^-	0.712 ; 0.002 ; 0.001	0.797 ; -0.680 ; -0.002	0.658 ; 0.013 ; 0.788	0.810 ; 0.789 ; -0.797	0.807 ; 0.809 ; 0.805
	PF_6^-	0.703; 0.001; 0.002	-0.001; 0.787; -0.668	0.787; 0.648; 0.011	0.773; -0.782; 0.793	0.790; 0.790; 0.789
β	CH_3COO^{-a}	0.001 ; 0.677 ; 0.001	-0.630 ; 0.002 ; 0.768	0.610 ; 0.008 ; 0.766	-0.763 ; 0.792 ; 0.736	0.762 ; 0.785 ; 0.753
	CH_3COO^{-b}	0.002 ; 0.661 ; -0.001	0.723 ; -0.609 ; 0.001	0.013 ; 0.744 ; 0.584	0.682 ; -0.743 ; 0.751	0.706 ; 0.749 ; 0.740
	NO_3^-	0.665 ; 0.000 ; 0.002	0.627 ; -0.001 ; -0.747	0.751 ; 0.599 ; 0.011	-0.747 ; 0.766 ; 0.712	0.753 ; 0.757 ; 0.733
	ClO_4^-	0.000 ; 0.001 ; 0.660	-0.001 ; -0.762 ; 0.626	0.010 ; 0.758 ; 0.601	0.736 ; -0.758 ; 0.760	0.756 ; 0.751 ; 0.750
	HSO_4^-	0.002 ; 0.653 ; 0.000	-0.001 ; -0.752 ; 0.609	0.010 ; 0.742 ; 0.592	-0.741 ; 0.756 ; 0.718	0.745 ; 0.746 ; 0.739
	$H_2PO_4^-$	0.673 ; -0.001 ; 0.002	-0.741 ; 0.599 ; -0.001	0.738 ; 0.573 ; 0.010	0.703 ; -0.736 ; 0.742	0.726 ; 0.741 ; 0.727
	F^-	0.671 ; 0.000 ; 0.001	0.001 ; 0.728 ; -0.601	0.009 ; 0.753 ; 0.550	0.694 ; -0.722 ; 0.728	0.715 ; 0.722 ; 0.709
	Cl^-	0.659 ; 0.000 ; 0.001	0.609 ; -0.001 ; -0.750	0.010 ; 0.744 ; 0.593	-0.739 ; 0.745 ; 0.725	0.745 ; 0.734 ; 0.748
	Br^-	0.661 ; 0.000 ; 0.001	0.753 ; -0.617 ; 0.001	0.010 ; 0.746 ; 0.595	-0.741 ; 0.748 ; 0.729	0.747 ; 0.737 ; 0.752
	I^-	0.667 ; 0.000 ; 0.001	0.001 ; 0.753 ; -0.624	0.010 ; 0.749 ; 0.601	-0.746 ; 0.749 ; 0.735	0.750 ; 0.740 ; 0.755
	PF_6^-	0.659; 0.000; 0.001	-0.758; 0.621; -0.001	0.755; 0.597; 0.009	-0.751; 0.764; 0.735	0.751; 0.753; 0.754

[a)] The methyl group is pointing inwards the binding pocket; and [b)] the carboxylate group is pointing inwards the binding pocket.

Table S6. Uncorrected electronic binding energies ($\Delta\mathcal{E}_0$),[a] Zero Point Corrections (ΔZPE),[b] thermal corrected binding energies (ΔE),[c] binding enthalpies (ΔH),[d] binding entropies term contribution ($T\Delta S$),[e] binding free energies (ΔG),[f] and standard state binding free energies (ΔG^{SS})[g] (in kcal mol^{-1}) for the oxo-anion associations of $\mathbf{1}^{n+}$.[h]

Oxidation state	Energy term	α pocket					β pocket					
		CH_3COO^-	NO_3^-	ClO_4^-	HSO_4^-	$H_2PO_4^-$	CH_3COO^{-i}	CH_3COO^{-j}	NO_3^-	ClO_4^-	HSO_4^-	$H_2PO_4^-$
	$\Delta\mathcal{E}_0$	-17.84	-15.56	-17.04	-19.61	-21.21	-10.57	-4.92	-6.06	-10.49	-9.92	-7.51
	ΔZPE	1.89	1.23	1.36	1.42	1.64	1.65	1.03	0.97	1.10	1.24	1.35
	ΔE	-15.62	-13.55	-14.86	-17.47	-19.04	-8.36	-3.06	-4.15	-8.57	-7.96	-5.51
$\mathbf{1}^{3+}$	ΔH	-16.21	-14.14	-15.45	-18.06	-19.63	-8.95	-3.65	-4.75	-9.16	-8.56	-6.10
	$T\Delta S$	-14.59	-12.52	-13.45	-13.76	-14.31	-14.10	-12.85	-12.24	-13.86	-14.57	-14.60
	ΔG	-1.62	-1.62	-2.00	-4.30	-5.32	5.15	9.20	7.49	4.70	6.01	8.51
	ΔG^{SS}	-3.51	-3.51	-3.89	-6.19	-7.21	3.26	7.31	5.60	2.81	4.12	6.62
	$\Delta\mathcal{E}_0$	-24.58	-20.44	-20.90	-24.41	-28.04	-12.63	-9.47	-10.08	-15.01	-15.38	-14.07
	ΔZPE	1.05	0.96	0.83	0.99	1.37	0.98	0.62	0.80	0.74	0.81	1.10
	ΔE	-22.88	-18.60	-19.08	-22.57	-26.09	-10.79	-7.92	-8.27	-13.26	-13.64	-12.18
$\mathbf{1}^{4+}$	ΔH	-23.48	-19.19	-19.67	-23.16	-26.68	-11.38	-8.51	-8.87	-13.86	-14.23	-12.78
	$T\Delta S$	-12.78	-12.13	-12.46	-13.09	-13.98	-12.48	-12.71	-12.06	-12.67	-13.11	-13.57
	ΔG	-10.70	-7.07	-7.21	-10.07	-12.70	1.10	4.20	3.20	-1.19	-1.11	0.80
	ΔG^{SS}	-12.59	-8.96	-9.10	-11.96	-14.59	-0.79	2.31	1.31	-3.08	-3.00	-1.09
	$\Delta\mathcal{E}_0$	-29.90	-25.12	-24.71	-29.53	-34.33	-15.18	-15.54	-14.95	-19.50	-20.64	-20.19
	ΔZPE	1.76	1.07	1.31	1.54	1.57	1.10	1.73	0.89	0.83	0.95	0.83
	ΔE	-27.80	-23.25	-22.59	-27.35	-32.28	-13.25	-13.29	-13.04	-17.69	-18.81	-18.36
ls-$\mathbf{1}^{5+}$	ΔH	-28.39	-23.85	-23.19	-27.94	-32.87	-13.84	-13.88	-13.64	-18.29	-19.40	-18.95
	$T\Delta S$	-14.29	-12.46	-13.56	-14.01	-14.22	-12.83	-14.52	-12.08	-12.89	-13.46	-13.11
	ΔG	-14.10	-11.39	-9.63	-13.93	-18.65	-1.01	0.64	-1.56	-5.39	-5.94	-5.84
	ΔG^{SS}	-15.99	-13.28	-11.52	-15.82	-20.54	-2.90	-1.25	-3.45	-7.28	-7.83	-7.73
	$\Delta\mathcal{E}_0$	-29.86	-25.06	-24.71	-29.84	-34.31	-15.15	-13.69	-14.49	-19.52	-20.67	-20.21
	ΔZPE	1.78	1.09	1.31	1.55	1.57	1.22	0.59	0.70	0.85	1.00	0.88
	ΔE	-27.75	-23.19	-22.59	-27.68	-32.26	-13.17	-12.16	-12.65	-17.70	-18.75	-18.36
hs-$\mathbf{1}^{5+}$	ΔH	-28.34	-23.79	-23.19	-28.27	-32.85	-13.76	-12.76	-13.25	-18.29	-19.35	-18.96
	$T\Delta S$	-14.35	-12.50	-13.67	-14.33	-14.36	-13.36	-12.63	-11.11	-12.89	-13.27	-13.30
	ΔG	-13.99	-11.28	-9.52	-13.94	-18.49	-0.40	-0.13	-2.14	-5.40	-6.07	-5.66
	ΔG^{SS}	-15.88	-13.17	-11.41	-15.83	-20.38	-2.29	-2.02	-4.03	-7.29	-7.96	-7.55
	$\Delta\mathcal{E}_0$	-36.78	-30.18	-28.43	-34.53	-40.52	-16.82	-20.72	-19.55	-24.01	-26.21	-26.70
	ΔZPE	1.88	1.51	0.95	1.23	1.29	2.00	1.44	1.26	1.16	1.19	1.15
	ΔE	-34.67	-28.15	-26.65	-32.69	-38.74	-14.32	-18.72	-17.41	-22.00	-24.22	-24.78
ls-$\mathbf{1}^{6+}$	ΔH	-35.26	-28.74	-27.24	-33.28	-39.33	-14.92	-19.31	-18.00	-22.59	-24.81	-25.38
	$T\Delta S$	-14.31	-13.56	-12.69	-13.94	-13.95	-13.86	-13.69	-11.87	-13.28	-13.52	-13.98
	ΔG	-20.95	-15.18	-14.55	-19.33	-25.38	-1.06	-5.62	-6.13	-9.32	-11.29	-11.40
	ΔG^{SS}	-22.84	-17.07	-16.44	-21.22	-27.27	-2.95	-7.51	-8.02	-11.21	-13.18	-13.29

Table S6. (continued)

	$\Delta\mathcal{E}_0$	-36.73	-30.07	-28.34	-34.41	-40.38	-16.80	-20.62	-19.48	-23.84	-26.17	-26.62
	ΔZPE	2.01	1.63	1.11	1.23	1.35	1.99	1.88	1.19	1.25	1.22	1.02
	ΔE	-34.56	-27.96	-26.47	-32.56	-38.56	-14.29	-18.35	-17.36	-21.77	-24.16	-24.76
hs-**1**$^{6+}$	ΔH	-35.15	-28.55	-27.06	-33.15	-39.15	-14.88	-18.94	-17.95	-22.37	-24.76	-25.35
	$T\Delta S$	-14.76	-13.67	-13.17	-13.66	-13.99	-13.33	-14.58	-11.45	-13.32	-13.43	-13.24
	ΔG	-20.40	-14.89	-13.89	-19.49	-25.15	-1.55	-4.37	-6.50	-9.05	-11.33	-12.11
	ΔG^{SS}	-22.29	-16.78	-15.78	-21.38	-27.04	-3.44	-6.26	-8.39	-10.94	-13.22	-14.00

[a] The energy values were not corrected for basis set superposition errors; [b] ΔZPE is included in the ΔE, ΔH and ΔG terms; [c] $\Delta E = \Delta\mathcal{E}_0 + \Delta E_{Tot}$, where ΔE_{Tot} accounts for the differences in the internal energy due to translational, rotational, vibrational and electronic motions; [d] $\Delta H = \Delta E + \Delta nRT$, where n is -1 for a 1:1 host-guest systems, R is the ideal gas constant and T is the temperature (298.15 K); [e] ΔS accounts for the differences in entropy due to in the translational, rotational, vibrational and electronic motions; [f] $\Delta G = \Delta H - T\Delta S$; [g] $\Delta G^{SS} = \Delta G + (-1.89 \text{ kcal mol}^{-1})$, which corresponds to the free energy change converting from the standard state at 1 atm (1 mol per 24.46 L) to 1 M (1 mol/L);[10] [h] the absolute energy terms are defined in the Detailed Methods section; [i] the methyl group is pointing inwards the binding pocket; and [j] the carboxylate group is pointing inwards the binding pocket.

Table S7. Average N···O and H···O distances (Å) and N–H···O angles (°) of the hydrogen bonds between $\mathbf{1}^{n+}$ and the α pocket hosted oxo-anions, computed from the DFT optimised structures.

Host	Parameter	CH_3COO^-	NO_3^-	ClO_4^-	HSO_4^-	$H_2PO_4^-$
$\mathbf{1}^{3+}$	N···O	3.003 ± 0.068	3.043 ± 0.060	3.112 ± 0.001	3.085 ± 0.026	3.014 ± 0.023
	H···O	2.093 ± 0.061	2.157 ± 0.048	2.233 ± 0.001	2.195 ± 0.025	2.107 ± 0.023
	N–H···O	148.2 ± 3.5	145.3 ± 3.0	144.5 ± 0.1	145.8 ± 1.2	147.8 ± 1.2
$\mathbf{1}^{4+}$	N···O	2.931 ± 0.041	2.997 ± 0.072	3.066 ± 0.011	3.034 ± 0.023	2.971 ± 0.050
	H···O	2.008 ± 0.020	2.103 ± 0.076	2.178 ± 0.008	2.134 ± 0.011	2.055 ± 0.065
	N–H···O	149.5 ± 3.3	146.4 ± 4.9	145.6 ± 2.4	147.0 ± 1.8	148.9 ± 4.0
ls-$\mathbf{1}^{5+}$	N···O	2.917 ± 0.102	2.923 ± 0.048	3.018 ± 0.016	2.987 ± 0.025	2.926 ± 0.023
	H···O	1.988 ± 0.105	2.019 ± 0.041	2.121 ± 0.006	2.077 ± 0.026	2.000 ± 0.034
	N–H···O	150.4 ± 5.8	147.2 ± 4.4	146.5 ± 1.8	148.0 ± 1.0	150.0 ± 1.9
hs-$\mathbf{1}^{5+}$	N···O	2.914 ± 0.096	2.923 ± 0.046	3.019 ± 0.019	2.985 ± 0.016	2.926 ± 0.023
	H···O	1.986 ± 0.098	2.020 ± 0.037	2.122 ± 0.009	2.076 ± 0.027	2.000 ± 0.034
	N–H···O	150.3 ± 5.6	147.1 ± 4.4	146.4 ± 1.8	148.0 ± 2.7	150.0 ± 1.9
ls-$\mathbf{1}^{6+}$	N···O	2.870 ± 0.093	2.879 ± 0.036	2.980 ± 0.004	2.951 ± 0.021	2.899 ± 0.020
	H···O	1.929 ± 0.087	1.965 ± 0.028	2.074 ± 0.004	2.032 ± 0.020	1.963 ± 0.021
	N–H···O	151.7 ± 3.9	148.2 ± 2.1	147.4 ± 0.1	149.1 ± 1.0	151.1 ± 0.8
hs-$\mathbf{1}^{6+}$	N···O	2.872 ± 0.095	2.880 ± 0.037	2.981 ± 0.003	2.953 ± 0.024	2.899 ± 0.021
	H···O	1.931 ± 0.090	1.965 ± 0.028	2.074 ± 0.002	2.033 ± 0.024	1.962 ± 0.021
	N–H···O	151.7 ± 3.8	148.3 ± 2.2	147.5 ± 0.2	149.1 ± 1.0	151.1 ± 0.9

Table S8. $A_c\cdots N_3$[a,b] distances (Å) between $\mathbf{1}^{n+}$ and the hosted oxo-anions in the DFT optimised structures.

Binding pocket	Host	CH_3COO^-	NO_3^-	ClO_4^-	HSO_4^-	$H_2PO_4^-$
α	$\mathbf{1}^{3+}$	3.616	3.677	4.036	3.975	3.917
	$\mathbf{1}^{4+}$	3.546	3.597	3.987	3.925	3.858
	ls-$\mathbf{1}^{5+}$	3.474	3.541	3.933	3.873	3.821
	hs-$\mathbf{1}^{5+}$	3.477	3.544	3.934	3.862	3.822
	ls-$\mathbf{1}^{6+}$	3.387	3.496	3.883	3.818	3.781
	hs-$\mathbf{1}^{6+}$	3.382	3.491	3.879	3.815	3.776
β	$\mathbf{1}^{3+}$	3.999[c]; 5.575[d]	4.888	4.878	4.953	5.206
	$\mathbf{1}^{4+}$	3.977[c]; 4.564[d]	4.567	4.627	4.623	4.804
	ls-$\mathbf{1}^{5+}$	3.888[c]; 4.266[d]	4.328	4.464	4.436	4.424
	hs-$\mathbf{1}^{5+}$	3.893[c]; 4.289[d]	4.277	4.464	4.441	4.425
	ls-$\mathbf{1}^{6+}$	4.015[c]; 4.062[d]	4.065	4.322	4.269	4.233
	hs-$\mathbf{1}^{6+}$	4.011[c]; 4.060[d]	4.062	4.317	4.256	4.221

[a] A_c denotes the anion's central atom, *i.e.*, A_c = S, P, N, Cl or C_{COO} in HSO_4^-, $H_2PO_4^-$, NO_3^-, ClO_4^- or CH_3COO^- anions, respectively; [b] the N_3 plane is determined by the three N atoms from the N–H groups of the 9MA bridging ligands; [c] A_c denotes the C_{Me} carbon atom; [d] A_c denotes the C_{COO^-} carbon atom.

Table S9. Average electron density (ρ, $e a_0^{-3}$), Laplacian of the density ($\nabla^2\rho$, $e a_0^{-3}$), potential energy density ($\mathcal{V}$, Hartrees), and energy of the hydrogen bonds (E_{HB}, kcal mol^{-1}) at the bond critical points in the N–H···O interactions between the $\mathbf{1}^{n+}$ hosts and oxo-anions hosted in the α pocket.[a]

Host	Parameter	CH_3COO^-	NO_3^-	ClO_4^-	HSO_4^-	$H_2PO_4^-$
$\mathbf{1}^{3+}$	ρ (×10)	0.19 ± 0.02	0.16 ± 0.01	0.13 ± 0.00	0.14 ± 0.00	0.18 ± 0.01
	$\nabla^2\rho$ (×10)	0.66 ± 0.10	0.58 ± 0.06	0.49 ± 0.00	0.54 ± 0.03	0.64 ± 0.03
	$\mathcal{V}$ (×10)	-0.16 ± 0.02	-0.13 ± 0.01	-0.11 ± 0.00	-0.12 ± 0.00	-0.15 ± 0.01
	E_{HB}	-5.02 ± 0.57	-4.12 ± 0.31	-3.33 ± 0.01	-3.77 ± 0.15	-4.79 ± 0.19
$\mathbf{1}^{4+}$	ρ (×10)	0.23 ± 0.01	0.18 ± 0.02	0.15 ± 0.00	0.16 ± 0.01	0.20 ± 0.02
	$\nabla^2\rho$ (×10)	0.78 ± 0.06	0.66 ± 0.10	0.55 ± 0.00	0.60 ± 0.02	0.72 ± 0.09
	$\mathcal{V}$ (×10)	-0.19 ± 0.01	-0.15 ± 0.02	-0.12 ± 0.00	-0.14 ± 0.01	-0.18 ± 0.02
	E_{HB}	-6.09 ± 0.24	-4.79 ± 0.60	-3.85 ± 0.06	-4.39 ± 0.16	-5.49 ± 0.64
ls-$\mathbf{1}^{5+}$	ρ (×10)	0.24 ± 0.04	0.21 ± 0.01	0.17 ± 0.00	0.19 ± 0.01	0.23 ± 0.01
	$\nabla^2\rho$ (×10)	0.84 ± 0.19	0.77 ± 0.07	0.61 ± 0.01	0.68 ± 0.04	0.80 ± 0.06
	$\mathcal{V}$ (×10)	-0.21 ± 0.04	-0.19 ± 0.01	-0.14 ± 0.00	-0.16 ± 0.01	-0.20 ± 0.01
	E_{HB}	-6.60 ± 1.23	-5.83 ± 0.36	-4.46 ± 0.12	-5.06 ± 0.29	-6.22 ± 0.41
hs-$\mathbf{1}^{5+}$	ρ (×10)	0.25 ± 0.04	0.21 ± 0.01	0.17 ± 0.00	0.19 ± 0.01	0.23 ± 0.01
	$\nabla^2\rho$ (×10)	0.84 ± 0.18	0.77 ± 0.06	0.61 ± 0.02	0.68 ± 0.04	0.80 ± 0.06
	$\mathcal{V}$ (×10)	-0.21 ± 0.04	-0.19 ± 0.01	-0.14 ± 0.00	-0.16 ± 0.01	-0.20 ± 0.01
	E_{HB}	-6.62 ± 1.16	-5.82 ± 0.33	-4.45 ± 0.14	-5.08 ± 0.20	-6.21 ± 0.42
ls-$\mathbf{1}^{6+}$	ρ (×10)	0.28 ± 0.03	0.24 ± 0.01	0.18 ± 0.00	0.21 ± 0.01	0.25 ± 0.01
	$\nabla^2\rho$ (×10)	0.94 ± 0.19	0.86 ± 0.06	0.67 ± 0.01	0.74 ± 0.04	0.86 ± 0.04
	$\mathcal{V}$ (×10)	-0.24 ± 0.04	-0.21 ± 0.01	-0.16 ± 0.00	-0.18 ± 0.01	-0.22 ± 0.01
	E_{HB}	-7.52 ± 1.12	-6.64 ± 0.29	-5.02 ± 0.04	-5.65 ± 0.19	-6.78 ± 0.26
hs-$\mathbf{1}^{6+}$	ρ (×10)	0.28 ± 0.03	0.24 ± 0.01	0.19 ± 0.00	0.21 ± 0.01	0.25 ± 0.01
	$\nabla^2\rho$ (×10)	0.94 ± 0.20	0.86 ± 0.06	0.67 ± 0.00	0.74 ± 0.04	0.86 ± 0.04
	$\mathcal{V}$ (×10)	-0.24 ± 0.04	-0.21 ± 0.01	-0.16 ± 0.00	-0.18 ± 0.01	-0.22 ± 0.01
	E_{HB}	-7.51 ± 1.15	-6.63 ± 0.28	-5.02 ± 0.01	-5.64 ± 0.23	-6.78 ± 0.26

[a] The assessed properties were averaged over the three N–H···O hydrogen bonds of the DFT optimised structures.

Table S10. 2nd-order perturbation (E^2) stabilisation energies of $n_O \rightarrow \sigma^*_{N-H}$[a] (kcal mol^{-1}) for the N–H···O interactions in the DFT optimised structures of the $\mathbf{1}^{n+}$ oxo-anions associations.

Host	CH_3COO^-	NO_3^-	ClO_4^-	HSO_4^-	$H_2PO_4^-$
$\mathbf{1}^{3+}$	25.42	18.00	12.25	15.40	22.90
$\mathbf{1}^{4+}$	34.62	17.25	15.43	19.63	28.43
ls-$\mathbf{1}^{5+}$	39.03	30.27	19.45	24.59	34.67
hs-$\mathbf{1}^{5+}$	39.25	30.23	19.47	24.67	34.67
ls-$\mathbf{1}^{6+}$	48.13	37.21	23.74	29.46	40.10
hs-$\mathbf{1}^{6+}$	48.04	37.27	23.85	29.42	40.38

[a] Considering the three N–H binding units together.

Table S11. X···N_3[a,b] distances (Å) between $\mathbf{1}^{n+}$ and the hosted halides in the DFT optimised structures.

Binding pocket	Host	F^-	Cl^-	Br^-	I^-
α	$\mathbf{1}^{3+}$	2.122	3.046	3.320	3.736
	$\mathbf{1}^{4+}$	2.084	2.935	3.207	3.600
	ls-$\mathbf{1}^{5+}$	2.031	2.842	3.098	3.482
	hs-$\mathbf{1}^{5+}$	2.033	2.845	3.101	3.474
	ls-$\mathbf{1}^{6+}$	1.986	2.773	3.008	3.380
	hs-$\mathbf{1}^{6+}$	1.980	2.771	3.007	3.380
β	$\mathbf{1}^{3+}$	5.449	5.534	5.729	5.783
	$\mathbf{1}^{4+}$	4.936	4.625	4.697	4.886
	ls-$\mathbf{1}^{5+}$	3.291	3.887	4.035	4.423
	hs-$\mathbf{1}^{5+}$	4.001	3.847	4.039	4.421
	ls-$\mathbf{1}^{6+}$	2.530	3.563	3.807	4.183
	hs-$\mathbf{1}^{6+}$	2.489	3.562	3.808	4.820

[a] X = F^-, Cl^-, Br^- or I^-; [b] the N_3 plane is determined by the three N atoms from the N–H groups of the 9MA bridging ligands.

Table S12. Uncorrected electronic binding energies ($\Delta\mathcal{E}_0$),[a] Zero Point Corrections (ΔZPE),[b] thermal corrected binding energies (ΔE),[c] binding enthalpies (ΔH),[d] binding entropies term contribution ($T\Delta S$),[e] binding free energies (ΔG),[f] and standard state binding free energies (ΔG^{SS})[g] (in kcal mol^{-1}) for the halide associations of $\mathbf{1}^{n+}$.[h]

Oxidation state	Energy term	α pocket				β pocket			
		F^-	Cl^-	Br^-	I^-	F^-	Cl^-	Br^-	I^-
$\mathbf{1}^{3+}$	$\Delta\mathcal{E}_0$	-17.78	-12.50	-12.70	-11.85	-2.31	-4.08	-4.71	-5.61
	ΔZPE	1.04	0.74	0.30	0.41	0.31	0.27	0.25	0.19
	ΔE	-16.92	-11.63	-12.04	-11.11	-1.41	-3.21	-3.83	-4.79
	ΔH	-17.51	-12.22	-12.63	-11.70	-2.01	-3.80	-4.42	-5.38
	$T\Delta S$	-9.67	-9.46	-8.76	-9.29	-6.65	-6.86	-7.12	-7.58
	ΔG	-7.84	-2.77	-3.87	-2.41	4.64	3.05	2.70	2.20
	ΔG^{SS}	-9.73	-4.66	-5.76	-4.30	2.75	1.16	0.81	0.31
$\mathbf{1}^{4+}$	$\Delta\mathcal{E}_0$	-27.38	-18.20	-17.42	-15.23	-4.69	-6.75	-7.75	-8.79
	ΔZPE	0.28	0.30	0.07	-0.14	0.14	0.06	-0.16	-0.16
	ΔE	-27.03	-17.65	-16.94	-14.84	-3.88	-5.99	-7.11	-8.13
	ΔH	-27.62	-18.24	-17.53	-15.43	-4.48	-6.59	-7.71	-8.72
	$T\Delta S$	-8.40	-8.83	-8.62	-8.28	-6.22	-6.61	-6.45	-6.43
	ΔG	-19.23	-9.42	-8.92	-7.15	1.74	0.03	-1.26	-2.30
	ΔG^{SS}	-21.12	-11.31	-10.81	-9.04	-0.15	-1.86	-3.15	-4.19
ls-$\mathbf{1}^{5+}$	$\Delta\mathcal{E}_0$	-36.21	-24.10	-22.39	-18.95	-8.02	-10.48	-11.70	-12.12
	ΔZPE	0.65	0.60	0.12	-0.02	-0.20	0.42	0.10	-0.04
	ΔE	-35.66	-23.37	-21.89	-18.47	-7.55	-9.50	-10.89	-11.43
	ΔH	-36.26	-23.97	-22.48	-19.06	-8.14	-10.09	-11.48	-12.02
	$T\Delta S$	-9.11	-9.27	-8.57	-8.47	-6.71	-7.18	-7.14	-7.39
	ΔG	-27.14	-14.70	-13.91	-10.59	-1.43	-2.91	-4.34	-4.63
	ΔG^{SS}	-29.03	-16.59	-15.80	-12.48	-3.32	-4.80	-6.23	-6.52
hs-$\mathbf{1}^{5+}$	$\Delta\mathcal{E}_0$	-36.11	-24.11	-22.40	-18.95	-7.44	-10.18	-11.46	-12.14
	ΔZPE	0.61	0.70	0.31	-0.14	0.23	-0.02	0.04	0.07
	ΔE	-35.60	-23.32	-21.76	-18.58	-6.66	-9.46	-10.73	-11.38
	ΔH	-36.19	-23.91	-22.35	-19.18	-7.25	-10.05	-11.33	-11.98
	$T\Delta S$	-9.18	-9.49	-8.97	-8.67	-7.32	-6.54	-7.41	-7.64
	ΔG	-27.01	-14.43	-13.39	-10.51	0.07	-3.51	-3.92	-4.34
	ΔG^{SS}	-28.90	-16.32	-15.28	-12.40	-1.82	-5.40	-5.81	-6.23
ls-$\mathbf{1}^{6+}$	$\Delta\mathcal{E}_0$	-44.73	-30.01	-27.47	-22.81	-14.63	-14.85	-15.86	-15.98
	ΔZPE	0.70	0.86	0.38	-0.13	-0.06	0.42	0.26	0.21
	ΔE	-44.32	-29.23	-26.91	-22.55	-14.18	-13.98	-15.06	-15.17
	ΔH	-44.91	-29.82	-27.50	-23.14	-14.77	-14.57	-15.65	-15.76
	$T\Delta S$	-9.64	-9.99	-9.49	-8.93	-7.01	-7.81	-7.83	-7.48
	ΔG	-35.27	-19.83	-18.02	-14.21	-7.76	-6.77	-7.82	-8.28
	ΔG^{SS}	-37.16	-21.72	-19.91	-16.10	-9.65	-8.66	-9.71	-10.17

Table S12. (continued)

	$\Delta\mathcal{E}_0$	-44.49	-29.82	-27.31	-22.69	-14.68	-14.77	-15.80	-15.95
	ΔZPE	0.78	0.95	0.44	-0.09	0.26	0.37	0.23	0.20
	ΔE	-44.00	-28.98	-26.71	-22.40	-14.02	-13.93	-15.02	-15.14
hs-**1**$^{6+}$	ΔH	-44.60	-29.57	-27.30	-23.00	-14.62	-14.52	-15.61	-15.73
	$T\Delta S$	-9.38	-9.93	-9.39	-8.82	-7.49	-7.52	-7.65	-7.40
	ΔG	-35.22	-19.64	-17.91	-14.18	-7.12	-7.01	-7.96	-8.33
	ΔG^{SS}	-37.11	-21.53	-19.80	-16.07	-9.01	-8.90	-9.85	-10.22

[a] The energy values were not corrected for basis set superposition errors ; [b] ΔZPE is included in the ΔE, ΔH and ΔG terms; [c] $\Delta E = \Delta\mathcal{E}_0 + \Delta E_{Tot}$, where ΔE_{Tot} accounts for the differences in the internal energy due to translational, rotational, vibrational and electronic motions; [d] $\Delta H = \Delta E + \Delta nRT$, where n is -1 for a 1:1 host-guest systems, R is the ideal gas constant and T is the temperature (298.15 K); [e] ΔS accounts for the differences in entropy due to in the translational, rotational, vibrational and electronic motions; [f] $\Delta G = \Delta H - T\Delta S$; [g] $\Delta G^{SS} = \Delta G + (-1.89 \text{ kcal mol}^{-1})$, which corresponds to the free energy change converting from the standard state at 1 atm (1 mol per 24.46 L) to 1 M (1 mol/L);[10] and [h] the absolute energy terms are defined in the Detailed Methods section.

Table S13. Average N···X and H···X distances (Å) and N–H···X angles (°) of the hydrogen bonds between $\mathbf{1}^{n+}$ and the α pocket hosted halides, computed from the DFT optimised structures.[a]

Host	Parameter	F^-	Cl^-	Br^-	I^-
$\mathbf{1}^{3+}$	N···X	2.764 ± 0.006	3.526 ± 0.004	3.769 ± 0.006	4.147 ± 0.001
	H···X	1.818 ± 0.006	2.635 ± 0.004	2.889 ± 0.006	3.280 ± 0.002
	N–H···X	152.1 ± 0.3	146.6 ± 0.2	145.7 ± 0.2	144.6 ± 0.1
$\mathbf{1}^{4+}$	N···X	2.732 ± 0.067	3.426 ± 0.006	3.668 ± 0.019	4.023 ± 0.029
	H···X	1.780 ± 0.086	2.520 ± 0.015	2.770 ± 0.016	3.136 ± 0.026
	N–H···X	152.8 ± 4.5	148.4 ± 1.7	147.7 ± 1.3	146.8 ± 0.9
ls-$\mathbf{1}^{5+}$	N···X	2.688 ± 0.035	3.347 ± 0.008	3.573 ± 0.017	3.919 ± 0.032
	H···X	1.726 ± 0.047	2.428 ± 0.009	2.661 ± 0.013	3.016 ± 0.026
	N–H···X	153.8 ± 3.0	149.9 ± 1.6	149.3 ± 1.3	148.6 ± 1.1
hs-$\mathbf{1}^{5+}$	N···X	2.687 ± 0.033	3.349 ± 0.014	3.575 ± 0.024	3.910 ± 0.025
	H···X	1.726 ± 0.044	2.430 ± 0.012	2.663 ± 0.020	3.007 ± 0.021
	N–H···X	153.7 ± 2.9	149.9 ± 1.3	149.3 ± 1.1	148.5 ± 1.0
ls-$\mathbf{1}^{6+}$	N···X	2.659 ± 0.005	3.293 ± 0.002	3.501 ± 0.004	3.833 ± 0.010
	H···X	1.688 ± 0.006	2.362 ± 0.003	2.576 ± 0.004	2.916 ± 0.010
	N–H···X	154.9 ± 0.1	151.4 ± 0.2	151.0 ± 0.3	150.3 ± 0.1
hs-$\mathbf{1}^{6+}$	N···X	2.659 ± 0.003	3.295 ± 0.002	3.503 ± 0.005	3.835 ± 0.010
	H···X	1.687 ± 0.003	2.364 ± 0.003	2.578 ± 0.006	2.918 ± 0.010
	N–H···X	155.0 ± 0.1	151.4 ± 0.2	151.0 ± 0.3	150.3 ± 0.1

[a] X = F^-, Cl^-, Br^- or I^-.

Table S14. Average electron density (ρ, $e a_0^{-3}$), Laplacian of the density ($\nabla^2\rho$, $e a_0^{-3}$), potential energy density ($\mathcal{V}$, Hartrees), and energy of the hydrogen bonds (E_{HB}, kcal mol^{-1}) at the bond critical points in the N–H···X[b] interactions between the $\mathbf{1}^{n+}$ hosts and halides hosted in the α pocket.[a]

Host	Parameter	F^-	Cl^-	Br^-	I^-
$\mathbf{1}^{3+}$	ρ (×10)	0.34 ± 0.00	0.11 ± 0.00	0.08 ± 0.00	0.05 ± 0.00
	$\nabla^2\rho$ (×10)	1.08 ± 0.02	0.36 ± 0.00	0.26 ± 0.00	0.15 ± 0.00
	$\mathcal{V}$ (×10)	-0.34 ± 0.00	-0.07 ± 0.00	-0.04 ± 0.00	-0.02 ± 0.00
	E_{HB}	-10.72 ± 0.16	-2.11 ± 0.02	-1.31 ± 0.02	-0.70 ± 0.00
$\mathbf{1}^{4+}$	ρ (×10)	0.38 ± 0.07	0.14 ± 0.00	0.10 ± 0.00	0.07 ± 0.00
	$\nabla^2\rho$ (×10)	1.22 ± 0.25	0.44 ± 0.01	0.32 ± 0.01	0.20 ± 0.01
	$\mathcal{V}$ (×10)	-0.38 ± 0.07	-0.09 ± 0.00	-0.06 ± 0.00	-0.03 ± 0.00
	E_{HB}	-11.95 ± 2.27	-2.85 ± 0.11	-1.80 ± 0.08	-0.99 ± 0.06
ls-$\mathbf{1}^{5+}$	ρ (×10)	0.42 ± 0.04	0.17 ± 0.00	0.13 ± 0.00	0.09 ± 0.00
	$\nabla^2\rho$ (×10)	1.37 ± 0.14	0.52 ± 0.01	0.39 ± 0.01	0.25 ± 0.01
	$\mathcal{V}$ (×10)	-0.43 ± 0.04	-0.12 ± 0.00	-0.08 ± 0.00	-0.04 ± 0.00
	E_{HB}	-13.40 ± 1.34	-3.63 ± 0.09	-2.42 ± 0.09	-1.33 ± 0.09
hs-$\mathbf{1}^{5+}$	ρ (×10)	0.42 ± 0.04	0.17 ± 0.00	0.13 ± 0.00	0.09 ± 0.00
	$\nabla^2\rho$ (×10)	1.37 ± 0.14	0.52 ± 0.01	0.39 ± 0.02	0.25 ± 0.01
	$\mathcal{V}$ (×10)	-0.43 ± 0.04	-0.11 ± 0.00	-0.08 ± 0.00	-0.04 ± 0.00
	E_{HB}	-13.39 ± 1.27	-3.61 ± 0.13	-2.41 ± 0.14	-1.36 ± 0.07
ls-$\mathbf{1}^{6+}$	ρ (×10)	0.46 ± 0.01	0.19 ± 0.00	0.15 ± 0.00	0.11 ± 0.00
	$\nabla^2\rho$ (×10)	1.49 ± 0.02	0.58 ± 0.00	0.45 ± 0.00	0.29 ± 0.00
	$\mathcal{V}$ (×10)	-0.46 ± 0.01	-0.14 ± 0.00	-0.10 ± 0.00	-0.05 ± 0.00
	E_{HB}	-14.59 ± 0.20	-4.30 ± 0.03	-3.04 ± 0.03	-1.71 ± 0.04
hs-$\mathbf{1}^{6+}$	ρ (×10)	0.46 ± 0.00	0.19 ± 0.00	0.15 ± 0.00	0.11 ± 0.00
	$\nabla^2\rho$ (×10)	1.50 ± 0.01	0.58 ± 0.00	0.44 ± 0.00	0.29 ± 0.00
	$\mathcal{V}$ (×10)	-0.46 ± 0.00	-0.14 ± 0.00	-0.10 ± 0.00	-0.05 ± 0.00
	E_{HB}	-14.59 ± 0.11	-4.28 ± 0.03	-3.02 ± 0.04	-1.70 ± 0.04

[a] The assessed properties were averaged over the three N–H···X hydrogen bonds of the DFT optimised structures; [b] X = F^-, Cl^-, Br^- or I^-.

Table S15. E^2 stabilisation energies of $n_X \rightarrow \sigma^*_{N-H}$[a] (kcal mol^{-1}) for the N–H···X[b] interactions in the DFT optimised structures of the $\mathbf{1}^{n+}$ halide associations.

Host	F^-	Cl^-	Br^-	I^-
$\mathbf{1}^{3+}$	56.91	12.62	8.12	4.13
$\mathbf{1}^{4+}$	68.41	19.04	12.4	6.95
ls-$\mathbf{1}^{5+}$	80.33	26.34	18.22	10.74
hs-$\mathbf{1}^{5+}$	80.08	26.12	18.11	10.98
ls-$\mathbf{1}^{6+}$	90.98	33.65	24.75	15.44
hs-$\mathbf{1}^{6+}$	91.15	33.56	24.65	15.34

[a] Considering the three N–H binding units together; [b] X = F^-, Cl^-, Br^- or I^-.

Table S16. HOMO energy values (eV) in the DFT optimised structures of free $\mathbf{1}^{n+}$ and their α pocket anion associations.

Anion	$\mathbf{1}^{3+}$	$\mathbf{1}^{4+}$	*ls*-$\mathbf{1}^{5+}$	*hs*-$\mathbf{1}^{5+}$	*ls*-$\mathbf{1}^{6+}$	*hs*-$\mathbf{1}^{6+}$
--	-6.81	-7.11	-7.67	-7.72	-8.92	-9.14
CH_3COO^-	-6.54	-6.84	-7.39	-7.45	-8.62	-8.84
NO_3^-	-6.59	-6.91	-7.46	-7.52	-8.72	-8.93
ClO_4^-	-6.64	-6.94	-7.52	-7.57	-8.76	-8.98
HSO_4^-	-6.58	-6.89	-7.46	-7.52	-8.72	-8.93
$H_2PO_4^-$	-6.52	-6.84	-7.41	-7.46	-8.65	-8.87
F^-	-6.41	-6.75	-7.31	-7.36	-8.55	-8.76
Cl^-	-6.56	-6.86	-7.42	-7.48	-8.66	-8.89
Br^-	-6.6	-6.89	-7.46	-7.52	-8.63	-8.64
I^-	-6.66	-6.95	-7.52	-7.57	-8.06	-8.06

Table S17. Adiabatic and Koopmans' theorem ionisation energies (IP_A and IP_K, respectively),[a] determined for the DFT optimised structures of free $\mathbf{1}^{n+}$ and their α pocket hosted anion associations.

Ionisation energies (eV)	IP_A			IP_K		
Host	$\mathbf{1}^{3+}$	$\mathbf{1}^{4+b}$	$\mathbf{1}^{5+c}$	$\mathbf{1}^{3+}$	$\mathbf{1}^{4+}$	$\mathbf{1}^{5+d}$
--	5.34	5.64 ; *5.64*	6.02 ; *6.06* ; <u>6.02</u> ; **6.06**	6.81	7.11	7.67 ; *7.72*
CH_3COO^-	5.05	5.41 ; *5.41*	5.72 ; *5.77* ; <u>5.72</u> ; **5.76**	6.54	6.84	7.39 ; *7.45*
NO_3^-	5.13	5.43 ; *5.44*	5.80 ; *5.85* ; <u>5.80</u> ; **5.85**	6.59	6.91	7.46 ; *7.52*
ClO_4^-	5.17	5.47 ; *5.47*	5.86 ; *5.91* ; <u>5.86</u> ; **5.90**	6.64	6.94	7.52 ; *7.57*
HSO_4^-	5.13	5.42 ; *5.40*	5.80 ; *5.85* ; <u>5.82</u> ; **5.86**	6.58	6.89	7.46 ; *7.52*
$H_2PO_4^-$	5.04	5.36 ; *5.37*	5.75 ; *5.80* ; <u>5.75</u> ; **5.80**	6.52	6.84	7.41 ; *7.46*
F^-	4.92	5.25 ; *5.26*	5.65 ; *5.70* ; <u>5.65</u> ; **5.70**	6.41	6.75	7.31 ; *7.36*
Cl^-	5.09	5.38 ; *5.38*	5.76 ; *5.82* ; <u>5.76</u> ; **5.81**	6.56	6.86	7.42 ; *7.48*
Br^-	5.13	5.42 ; *5.42*	5.80 ; *5.85* ; <u>5.80</u> ; **5.85**	6.60	6.89	7.46 ; *7.52*
I^-	5.19	5.48 ; *5.48*	5.85 ; *5.90* ; <u>5.85</u> ; **5.90**	6.66	6.95	7.52 ; *7.57*

[a] Ionisation energies determined as $IP_A = \mathcal{E}_0^{(n+1)+} - \mathcal{E}_0^{n+}$, with n ranging from 3 to 5, and $IP_K = -E_{HOMO}$; [b] unformatted values for $IP_A = \mathcal{E}_0(ls\text{-}\mathbf{1}^{5+}) - \mathcal{E}_0(\mathbf{1}^{4+})$ and *italic* values for $IP_A = \mathcal{E}_0(hs\text{-}\mathbf{1}^{5+}) - \mathcal{E}_0(\mathbf{1}^{4+})$; [c] unformatted values for $IP_A = \mathcal{E}_0(ls\text{-}\mathbf{1}^{6+}) - \mathcal{E}_0(ls\text{-}\mathbf{1}^{5+})$, *italic* values for $IP_A = \mathcal{E}_0(hs\text{-}\mathbf{1}^{6+}) - \mathcal{E}_0(ls\text{-}\mathbf{1}^{5+})$, <u>underlined</u> values for $IP_A = \mathcal{E}_0(ls\text{-}\mathbf{1}^{6+}) - \mathcal{E}_0(hs\text{-}\mathbf{1}^{5+})$ and **bold** values for $IP_A = \mathcal{E}_0(hs\text{-}\mathbf{1}^{6+}) - \mathcal{E}_0(hs\text{-}\mathbf{1}^{5+})$; [d] unformatted values for $IP_K = -E_{HOMO}(ls\text{-}\mathbf{1}^{5+})$ and *italic* values for $IP_K = -E_{HOMO}(hs\text{-}\mathbf{1}^{5+})$.

Table S18. Comparison of the hydrogen bonding dimensions (distances in Å and angles in °) and the P···N_3 distances (Å) observed in the crystal structure of $\mathbf{1}^{3+}\cdot PF_6^-$ and in the DFT optimised structures of $\mathbf{1}^{n+}\cdot PF_6^-$ associations.[a]

Host	Parameter	X-Ray		DFT		
		α pocket	β pocket	α pocket	β pocket	α & β pocket (1:2)
$\mathbf{1}^{3+}$	N···F	3.623 ± 0.243	–	3.142 ± 0.006	–	3.173 ± 0.010
	H···F	2.832 ± 0.252	–	2.404 ± 0.006	–	2.440 ± 0.012
	N–H···F	152.1 ± 9.6	–	129.0 ± 0.1	–	128.6 ± 0.5
	P···N_3	4.504	5.986	4.048	5.128	4.078 (α) ; 5.379 (β)
$\mathbf{1}^{4+}$	N···F	–	–	3.086 ± 0.018	–	–
	H···F	–	–	2.319 ± 0.032	–	–
	N–H···F	–	–	131.5 ± 1.7	–	–
	P···N_3	–	–	3.997	4.958	–
ls-$\mathbf{1}^{5+}$	N···F	–	–	3.036 ± 0.021	–	–
	H···F	–	–	2.245 ± 0.035	–	–
	N–H···F	–	–	133.6 ± 1.6	–	–
	P···N_3	–	–	3.955	4.799	–
hs-$\mathbf{1}^{5+}$	N···F	–	–	3.057 ± 0.024	–	–
	H···F	–	–	2.266 ± 0.040	–	–
	N–H···F	–	–	133.9 ± 2.2	–	–
	P···N_3	–	–	3.976	4.799	–
ls-$\mathbf{1}^{6+}$	N···F	–	–	2.995 ± 0.004	–	–
	H···F	–	–	2.174 ± 0.008	–	–
	N–H···F	–	–	136.7 ± 0.8	–	–
	P···N_3	–	–	3.920	4.699	–
hs-$\mathbf{1}^{6+}$	N···F	–	–	2.994 ± 0.005	–	–
	H···F	–	–	2.173 ± 0.008	–	–
	N–H···F	–	–	136.8 ± 0.8	–	–
	P···N_3	–	–	3.918	4.700	–

[a] the N_3 plane is determined by the three N atoms from the N–H groups of the 9MA bridging ligands.

Table S19. Uncorrected electronic binding energies ($\Delta\mathcal{E}_0$),[a] Zero Point Corrections (ΔZPE),[b] thermal corrected binding energies (ΔE),[c] binding enthalpies (ΔH),[d] binding entropies term contribution ($T\Delta S$),[e] binding free energies (ΔG),[f] and standard state binding free energies (ΔG^{SS})[g] (in kcal mol^{-1}) for the PF_6^- associations of $\mathbf{1}^{n+}$.[h]

Binding pocket	Oxidation state	$\Delta\mathcal{E}_0$	ΔZPE	ΔE	ΔH	$T\Delta S$	ΔG	ΔG^{SS}
α	$\mathbf{1}^{3+}$	-12.79	1.37	-10.52	-11.11	-13.56	2.44	0.55
	$\mathbf{1}^{4+}$	-15.54	1.04	-13.46	-14.05	-12.83	-1.22	-3.11
	ls-$\mathbf{1}^{5+}$	-18.48	1.26	-16.30	-16.90	-13.64	-3.25	-5.14
	hs-$\mathbf{1}^{5+}$	-18.46	1.37	-16.17	-16.76	-13.74	-3.02	-4.91
	ls-$\mathbf{1}^{6+}$	-21.58	0.89	-19.72	-20.31	-13.17	-7.14	-9.03
	hs-$\mathbf{1}^{6+}$	-21.63	0.99	-19.70	-20.29	-13.21	-7.08	-8.97
β	$\mathbf{1}^{3+}$	-9.48	1.05	-7.53	-8.13	-13.93	5.80	3.91
	$\mathbf{1}^{4+}$	-14.00	0.73	-12.19	-12.78	-12.81	0.03	-1.87
	ls-$\mathbf{1}^{5+}$	-18.43	0.98	-16.38	-16.97	-12.94	-4.03	-5.92
	hs-$\mathbf{1}^{5+}$	-18.43	1.02	-16.37	-16.96	-13.07	-3.90	-5.79
	ls-$\mathbf{1}^{6+}$	-22.52	1.19	-20.44	-21.04	-13.29	-7.75	-9.64
	hs-$\mathbf{1}^{6+}$	-22.56	1.32	-20.42	-21.02	-13.75	-7.27	-9.16
α & β pocket (1:2)	$\mathbf{1}^{3+}$	-21.06	2.46	-16.82	-18.01	-27.76	9.75	7.86

[a] The energy values were not corrected for basis set superposition errors ; [b] ΔZPE is included in the ΔE, ΔH and ΔG terms; [c] $\Delta E = \Delta\mathcal{E}_0 + \Delta E_{Tot}$, where ΔE_{Tot} accounts for the differences in the internal energy due to translational, rotational, vibrational and electronic motions; [d] $\Delta H = \Delta E + \Delta nRT$, where n is -1 for a 1:1 host-guest systems, R is the ideal gas constant and T is the temperature (298.15 K); [e] ΔS accounts for the differences in entropy due to in the translational, rotational, vibrational and electronic motions; [f] $\Delta G = \Delta H - T\Delta S$; [g] $\Delta G^{SS} = \Delta G + (-1.89$ kcal mol^{-1}), which corresponds to the free energy change converting from the standard state at 1 atm (1 mol per 24.46 L) to 1 M (1 mol/L);[10] and [h] the absolute energy terms are defined in the Detailed Methods section.

Table S20. Average electron density (ρ, ea_0^{-3}), Laplacian of the density ($\nabla^2\rho$, ea_0^{-3}), potential energy density ($\mathcal{V}$, Hartrees), and energy of the hydrogen bonds (E_{HB}, kcal mol^{-1}) at the bond critical points in the N–H···F interactions between the $\mathbf{1}^{n+}$ hosts and PF_6^- in the α pocket,[a] together with the E^2 stabilisation energies of $n_F \rightarrow \sigma^*_{N-H}$ (kcal mol^{-1})[b] between $\mathbf{1}^{n+}$ and PF_6^-.

Host	ρ (×10)	$\nabla^2\rho$ (×10)	$\mathcal{V}$ (×10)	E_{HB}	E^2
$\mathbf{1}^{3+}$	0.08 ± 0.00	0.39 ± 0.00	-0.07 ± 0.00	-2.190 ± 0.038	4.17
$\mathbf{1}^{4+}$	0.10 ± 0.01	0.45 ± 0.02	-0.09 ± 0.01	-2.784 ± 0.220	6.28
ls-$\mathbf{1}^{5+}$	0.12 ± 0.01	0.51 ± 0.03	-0.11 ± 0.01	-3.405 ± 0.284	8.86
ls-$\mathbf{1}^{5+}$	0.11 ± 0.01	0.49 ± 0.03	-0.10 ± 0.01	-3.213 ± 0.333	8.24
ls-$\mathbf{1}^{6+}$	0.14 ± 0.00	0.56 ± 0.01	-0.13 ± 0.00	-4.082 ± 0.073	10.83
hs-$\mathbf{1}^{6+}$	0.14 ± 0.00	0.56 ± 0.01	-0.13 ± 0.00	-4.090 ± 0.075	10.92

[a] The assessed properties were averaged over the three N–H···O hydrogen bonds; [b] considering the three N–H binding units together.

Supplementary Figures

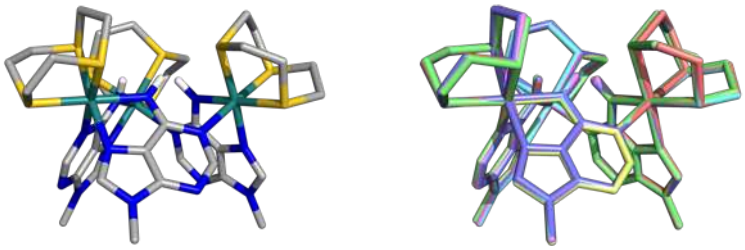

$\mathbf{1}^{3+}$ $\mathbf{1}^{n+}$

Fig. S11. DFT optimised structure of free $\mathbf{1}^{3+}$, together with the overlap of the optimised structures of $\mathbf{1}^{n+}$ in the four oxidation states and spin multiplicities, showing the structural similarities between them ($\mathbf{1}^{3+}$ – red; $\mathbf{1}^{4+}$ – green; *ls*-$\mathbf{1}^{5+}$ – blue; *hs*-$\mathbf{1}^{5+}$ – yellow; *ls*-$\mathbf{1}^{6+}$ – magenta; and *hs*-$\mathbf{1}^{6+}$ – cyan). The C–H hydrogen atoms were hidden for clarity.

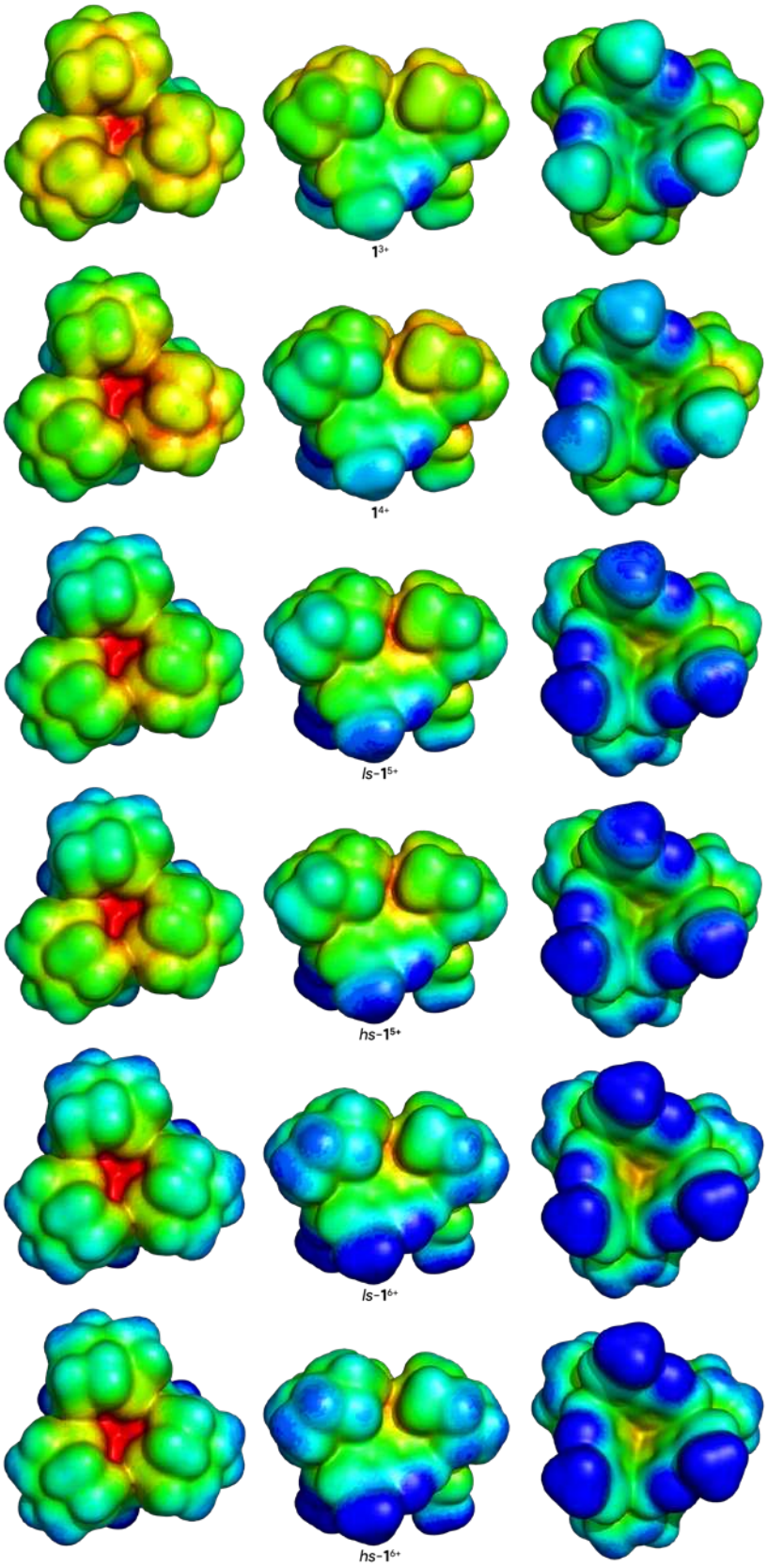

Fig. S12. Distribution of the electrostatic potential mapped on the 0.001 ea_0^{-3} isodensity surface of $\mathbf{1}^{n+}$, in the top (left), side (centre) and bottom views (right). The blue to red colour scales, in kcal mol^{-1}, range from 85 to 195 ($\mathbf{1}^{3+}$), from 140 to 250 ($\mathbf{1}^{4+}$), from 205 to 315 ($\mathbf{1}^{5+}$), and from 265 to 375 ($\mathbf{1}^{6+}$).

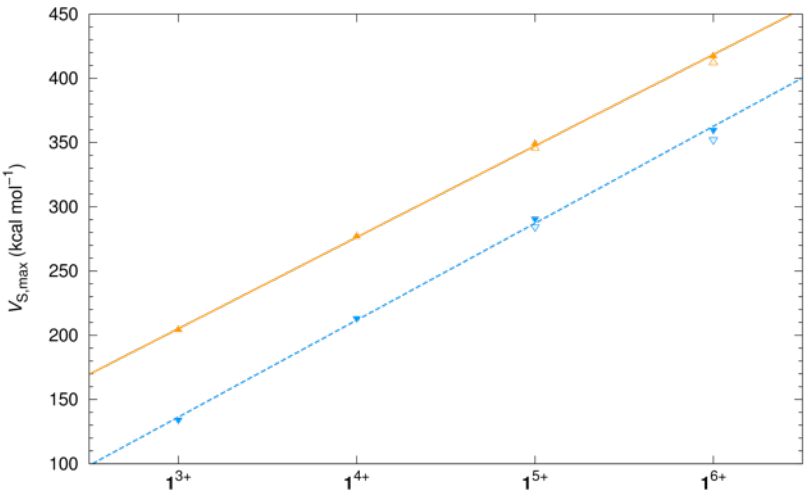

Fig. S13. Highest V_S values (kcal mol^{-1}) in the α (▲) and β pockets (▼) of $\mathbf{1}^{n+}$ *vs*. its oxidation state, together with their linear fits ($R^2 \geq 0.999$), calculated for the DFT optimised structures of the free hosts. The high-spin electron configurations of the $\mathbf{1}^{5+}$ and $\mathbf{1}^{6+}$ hosts are represented by the open points △ and ▽, respectively.

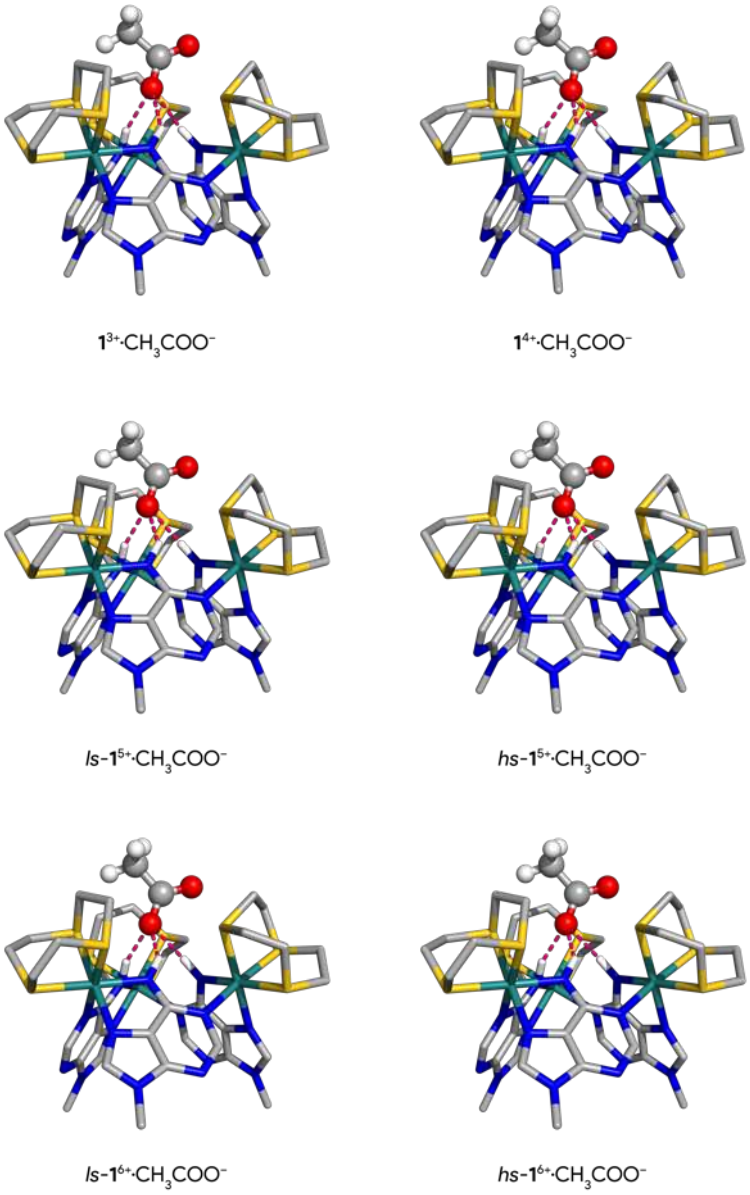

Fig. S14. DFT optimised structures of the $\mathbf{1}^{n+}\cdot CH_3COO^-$ associations, with the anion hosted in the α pocket. The N–H···O hydrogen bonds are drawn as pink dashed lines. The hosts' C–H hydrogen atoms were hidden for clarity.

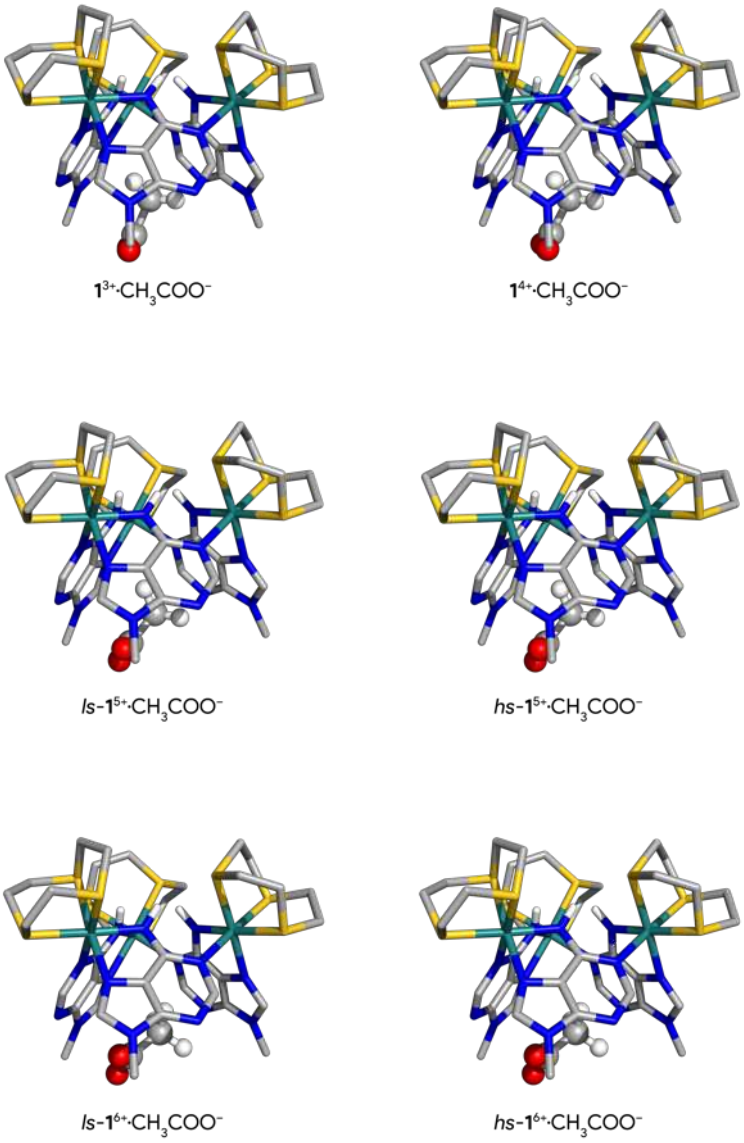

Fig. S15. DFT optimised structures of the $\mathbf{1}^{n+}\cdot CH_3COO^-$ associations, with the anion hosted in the β pocket and its methyl group pointing inwards the cavity. The hosts' C–H hydrogen atoms were hidden for clarity.

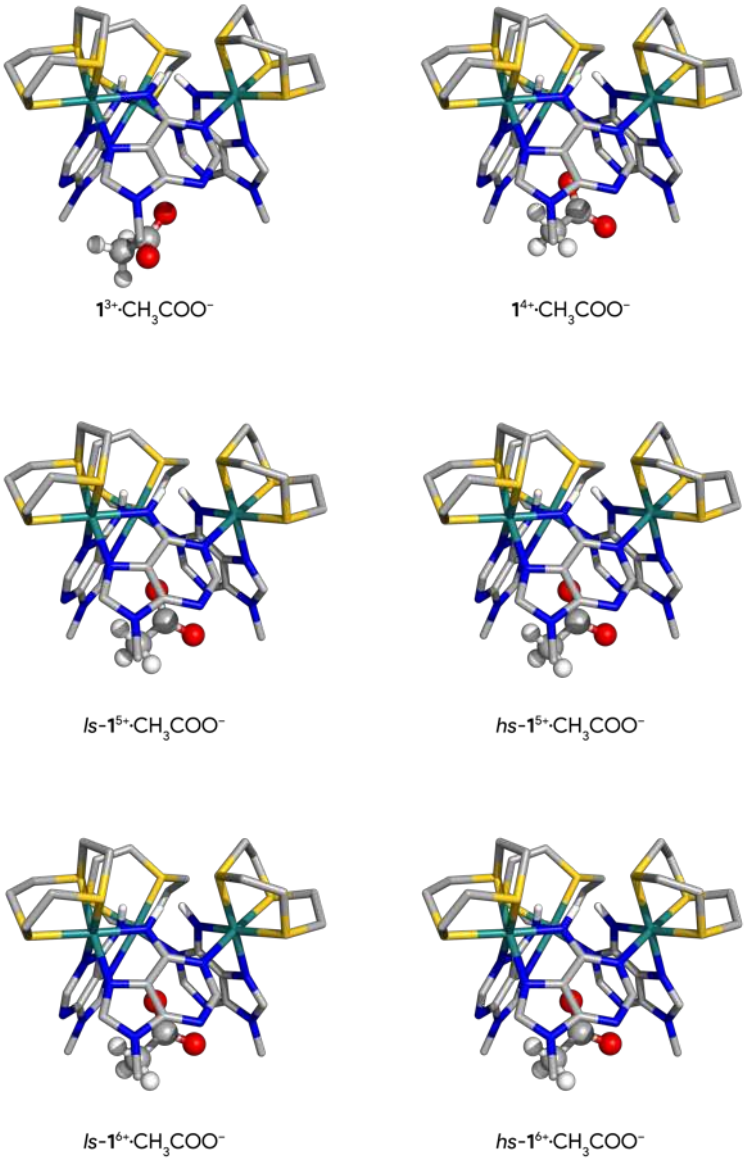

Fig. S16. DFT optimised structures of the $\mathbf{1}^{n+}\cdot CH_3COO^-$ associations, with the anion hosted in the β pocket and its carboxylate group pointing inwards the cavity. The hosts' C–H hydrogen atoms were hidden for clarity.

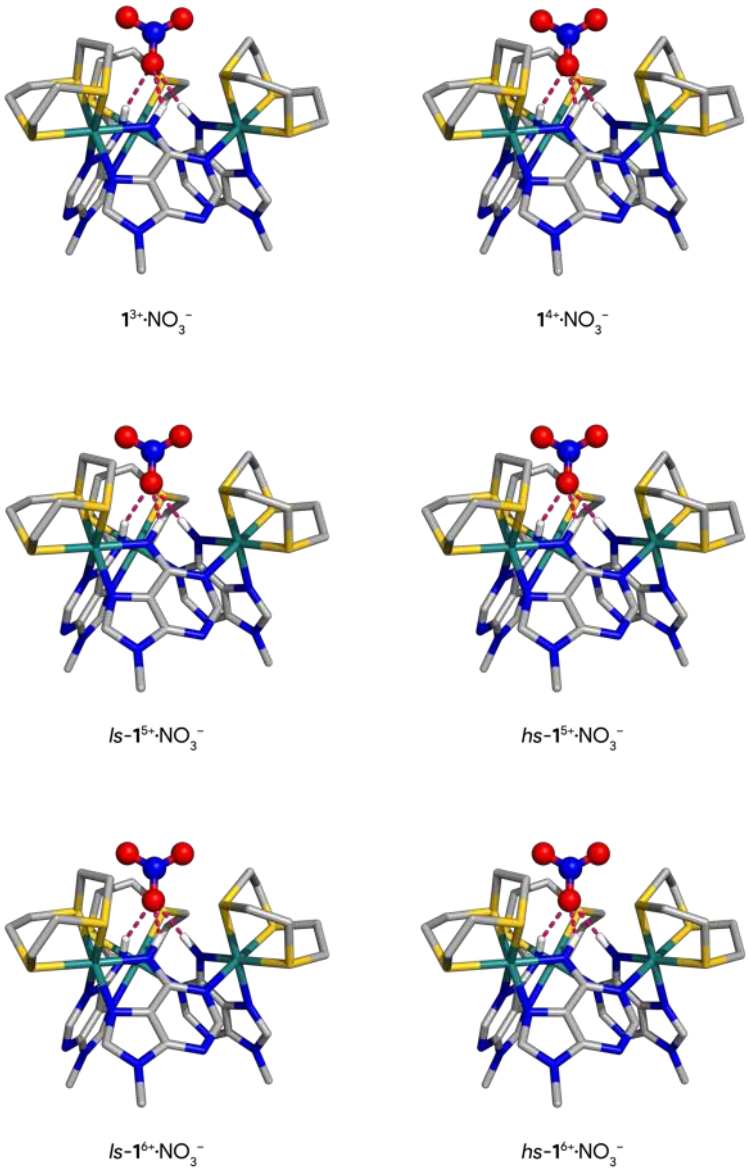

Fig. S17. DFT optimised structures of the $\mathbf{1}^{n+}\cdot NO_3^-$ associations, with the anion hosted in the α pocket. The N–H···O hydrogen bonds are drawn as pink dashed lines. The hosts' C–H hydrogen atoms were hidden for clarity.

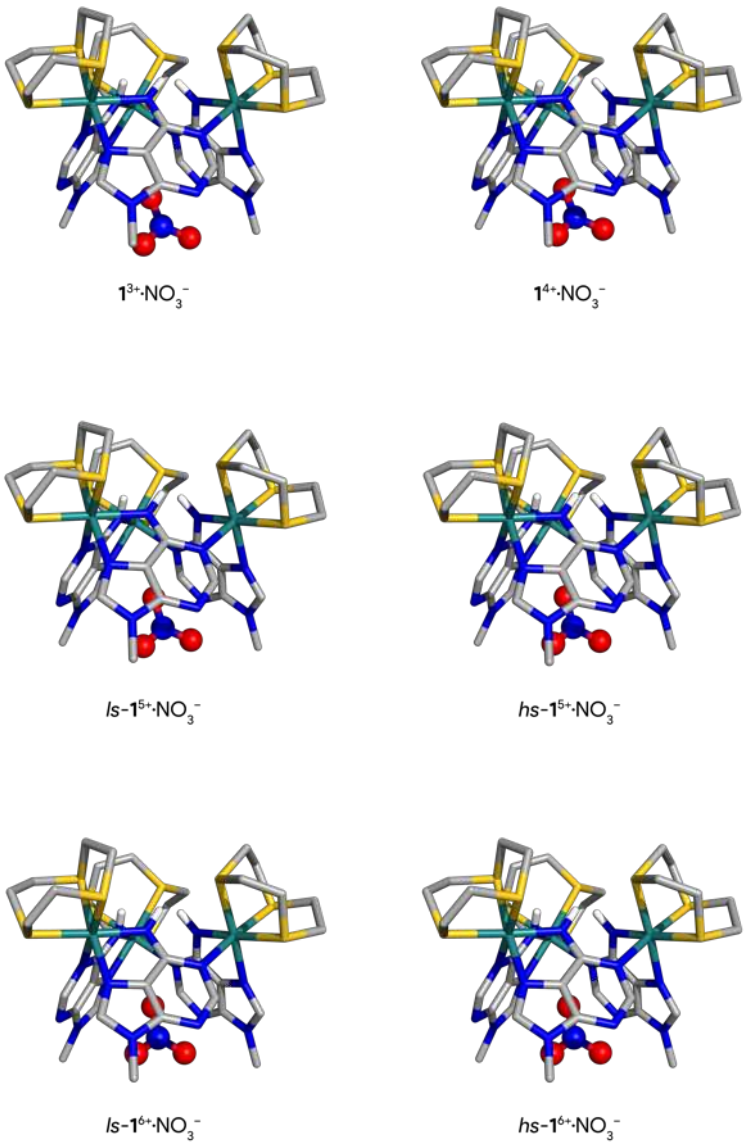

Fig. S18. DFT optimised structures of the $\mathbf{1}^{n+}\cdot NO_3^-$ associations, with the anion hosted in the β pocket. The hosts' C–H hydrogen atoms were hidden for clarity.

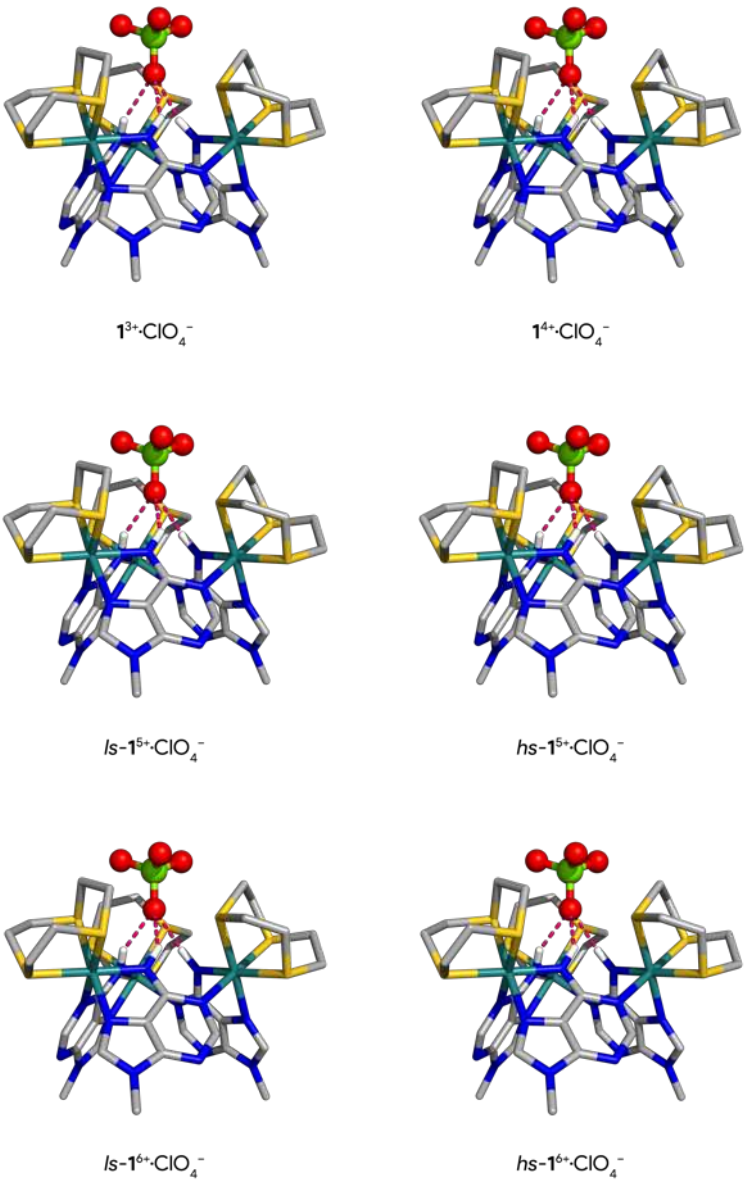

Fig. S19. DFT optimised structures of the $\mathbf{1}^{n+}\cdot ClO_4^-$ associations, with the anion hosted in the α pocket. The N–H···O hydrogen bonds are drawn as pink dashed lines. The hosts' C–H hydrogen atoms were hidden for clarity.

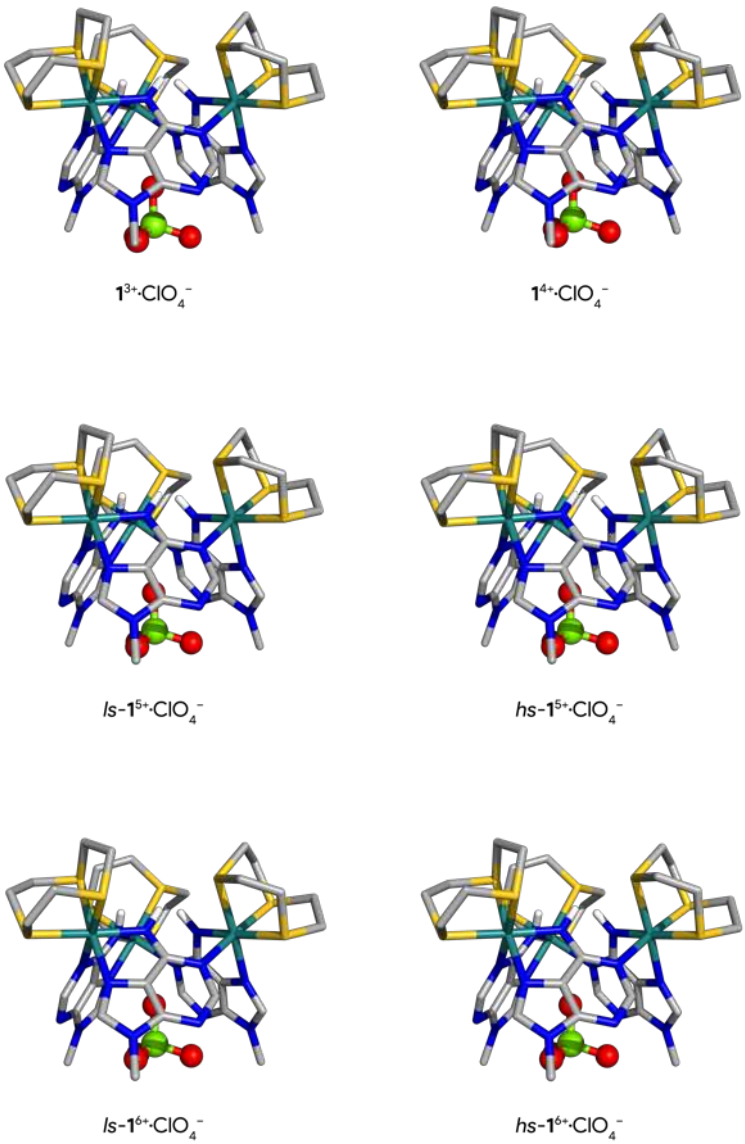

Fig. S20. DFT optimised structures of the $\mathbf{1}^{n+}\cdot ClO_4^-$ associations, with the anion hosted in the β pocket. The hosts' C–H hydrogen atoms were hidden for clarity.

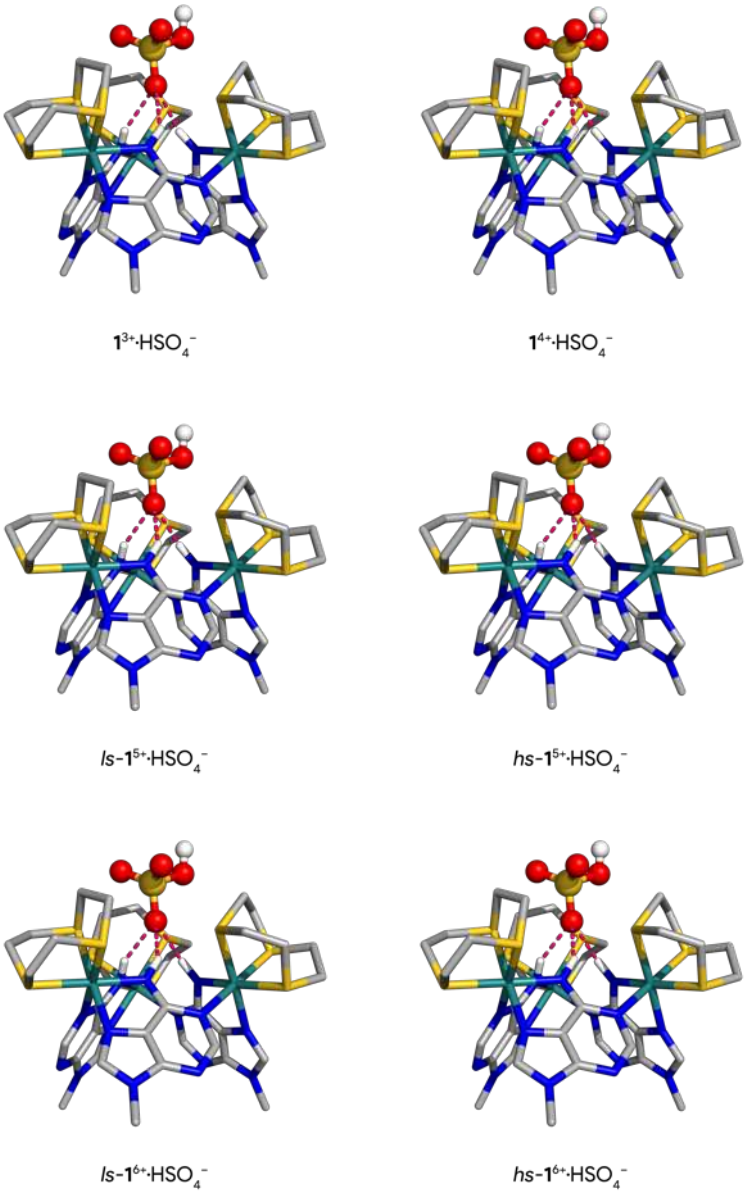

Fig. S21. DFT optimised structures of the $\mathbf{1}^{n+}\cdot HSO_4^-$ associations, with the anion hosted in the α pocket. The N–H···O hydrogen bonds are drawn as pink dashed lines. The hosts' C–H hydrogen atoms were hidden for clarity.

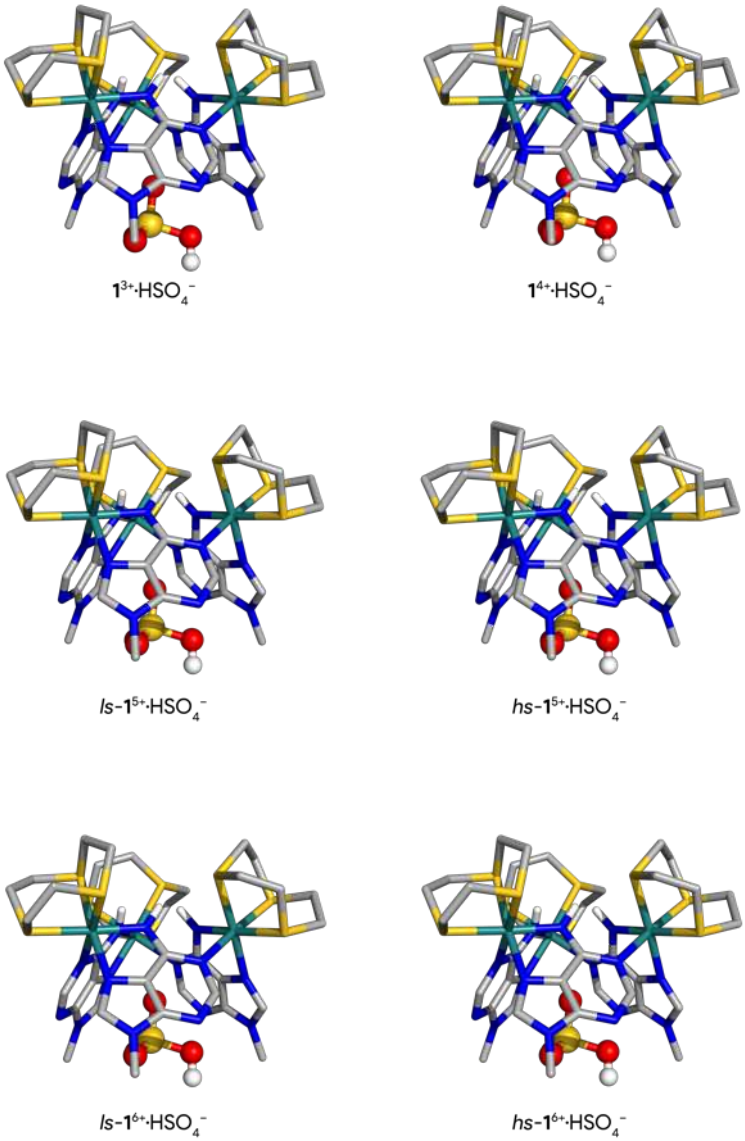

Fig. S22. DFT optimised structures of the $\mathbf{1}^{n+}\cdot HSO_4^-$ associations, with the anion hosted in the β pocket. The hosts' C–H hydrogen atoms were hidden for clarity.

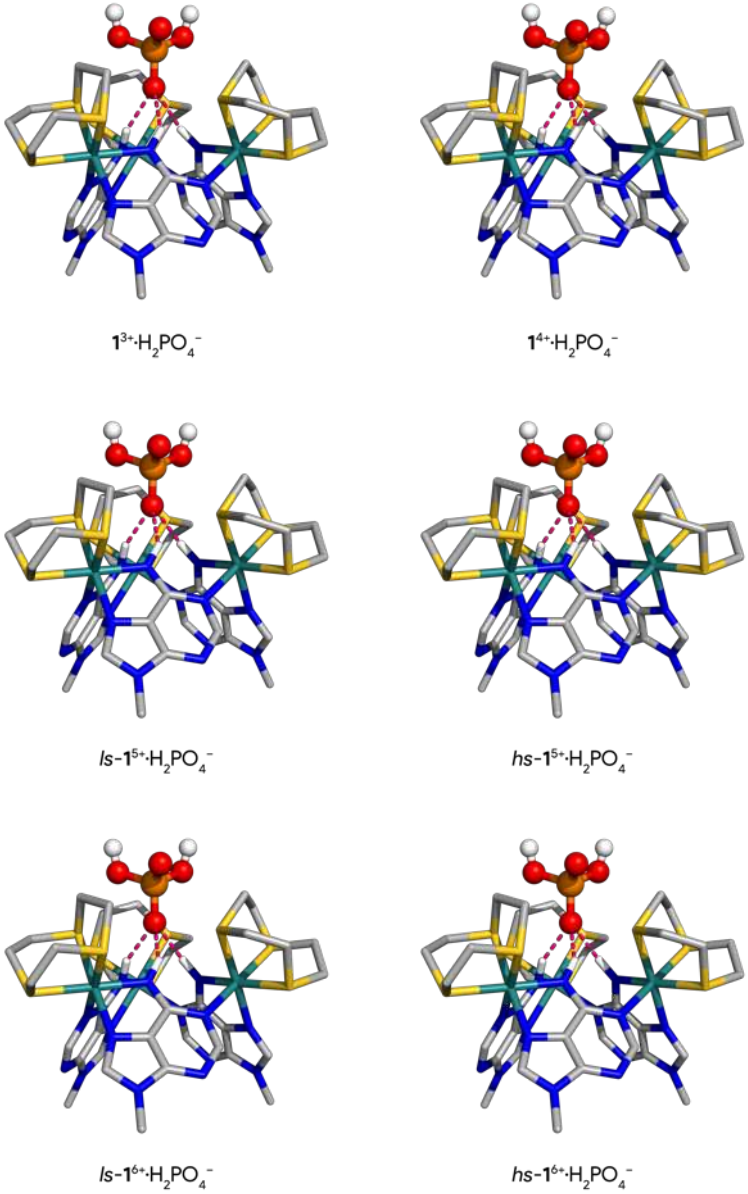

Fig. S23. DFT optimised structures of the $\mathbf{1}^{n+}\cdot H_2PO_4^-$ associations, with the anion hosted in the α pocket. The N–H···O hydrogen bonds are drawn as pink dashed lines. The hosts' C–H hydrogen atoms were hidden for clarity.

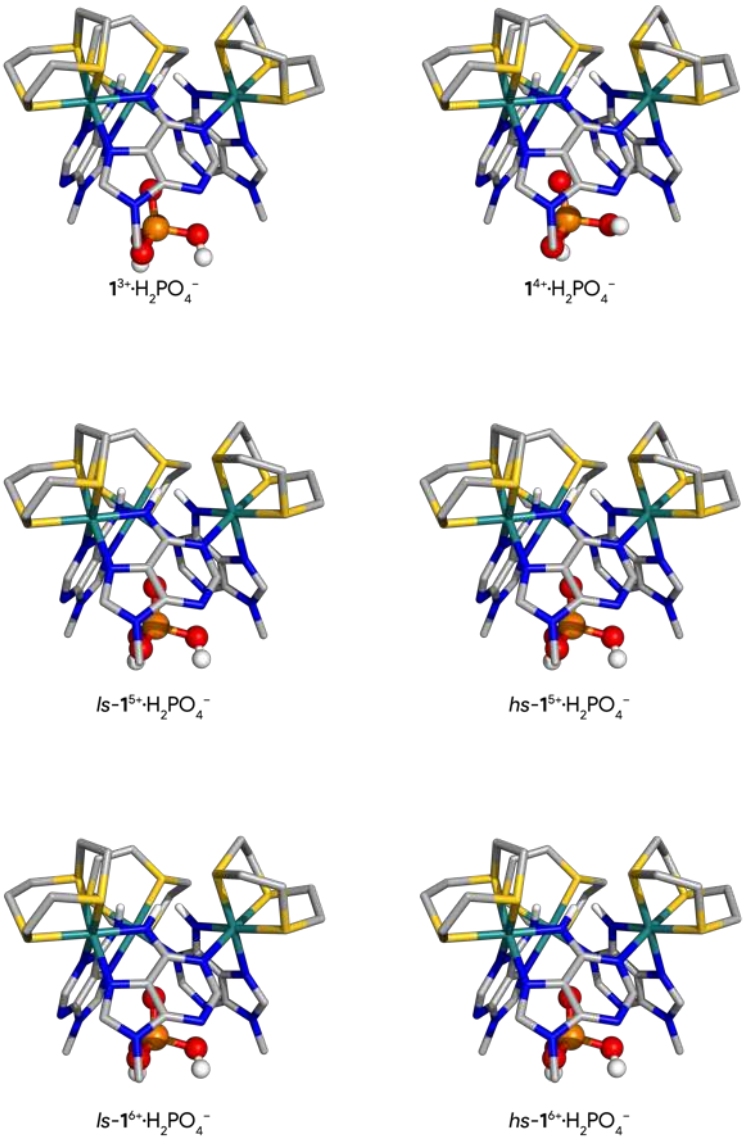

Fig. S24. DFT optimised structures of the $\mathbf{1}^{n+}\cdot H_2PO_4^-$ associations, with the anion hosted in the β pocket. The hosts' C–H hydrogen atoms were hidden for clarity.

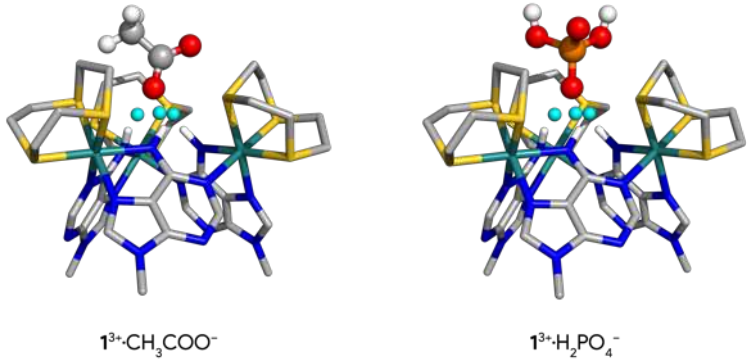

Fig. S25. Bond critical points (light blue spheres) of the N–H···O hydrogen bonds in the DFT optimised structures of $\mathbf{1}^{3+}$·CH_3COO^- and $\mathbf{1}^{3+}$·$H_2PO_4^-$. The hosts' C–H hydrogen atoms were hidden for clarity.

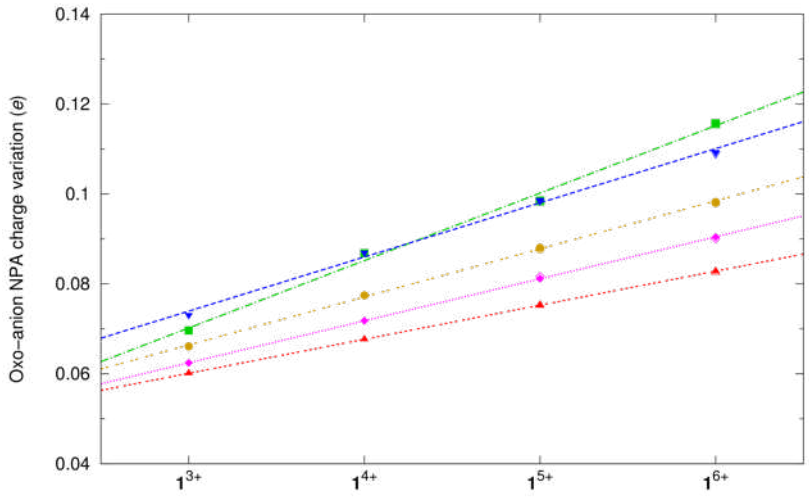

Fig. S26. Change in oxo-anion net charge (*e*) when hydrogen bonded to $\mathbf{1}^{n+}$ in the DFT optimised structures, together with the corresponding linear fits ($R^2 \geq 0.995$). Key: CH_3COO^- (■), NO_3^- (●), ClO_4^- (▲), HSO_4^- (◆) or $H_2PO_4^-$ (▼). The high-spin electron configurations are represented by the open points (□, ○, △, ◇ and ▽), but they might overlap with the low-spin points, as some charge variations are comparable between both spin multiplicities.

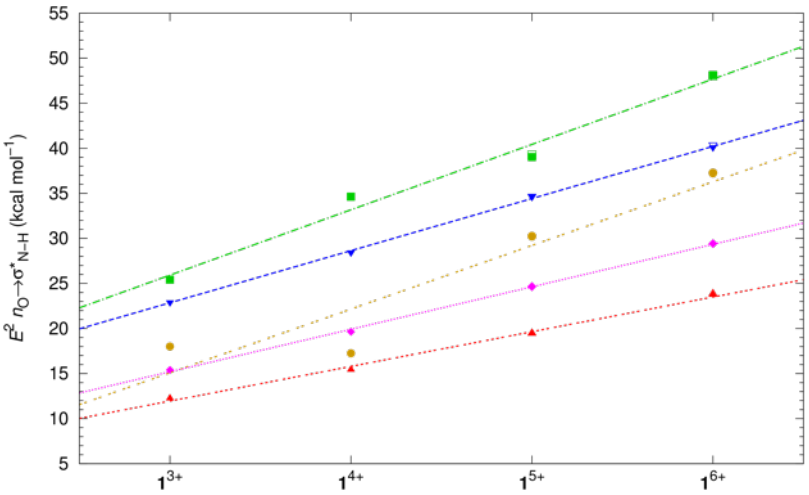

Fig. S27. Variation of the E^2 stabilisation energies of $n_O \rightarrow \sigma^*_{N-H}$ (kcal mol^{-1}) for N–H···O interactions in the DFT optimised structures of the $\mathbf{1}^{n+}$ oxo-anion associations, together with the corresponding linear fits ($R^2 \geq 0.879$). Key: CH_3COO^- (■), NO_3^- (●), ClO_4^- (▲), HSO_4^- (◆) or $H_2PO_4^-$ (▼). The high-spin electron configurations are represented by the open points (□, ○, △, ◇ and ▽), but they might overlap with the low-spin points, as E^2 energies are comparable between both spin multiplicities.

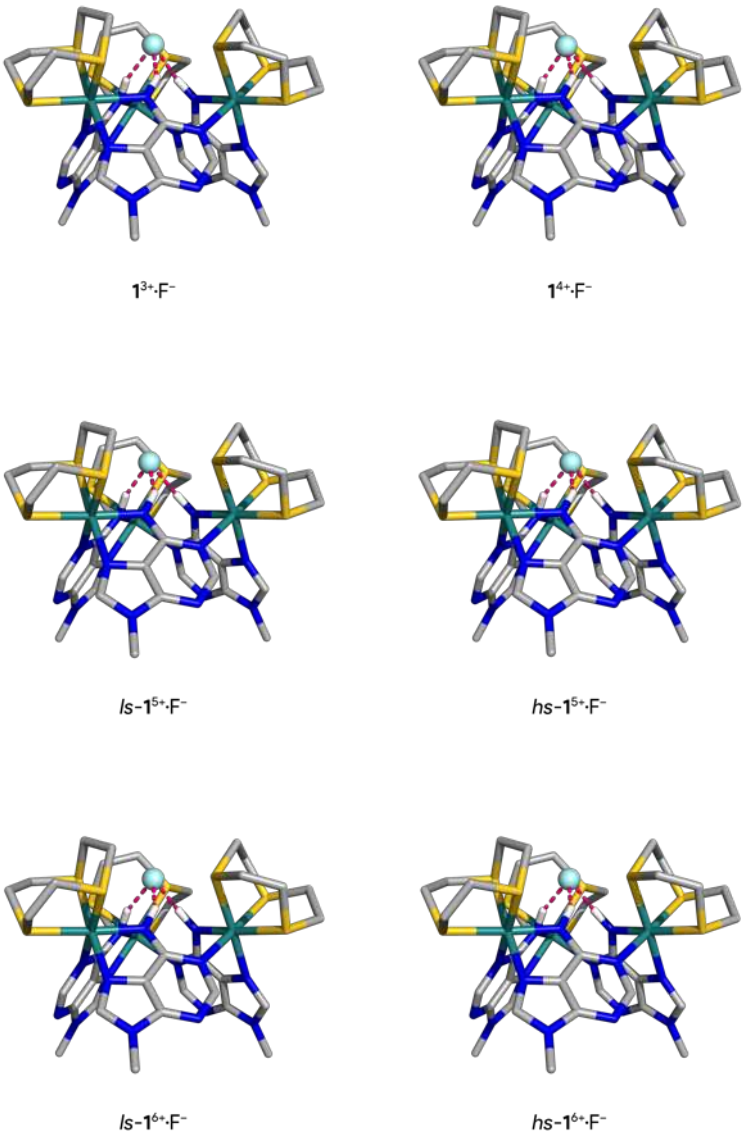

Fig. S28. DFT optimised structures of the $\mathbf{1}^{n+}\cdot F^-$ associations, with the anion hosted in the α pocket. The N–H···F^- hydrogen bonds are drawn as pink dashed lines. The hosts' C–H hydrogen atoms were hidden for clarity.

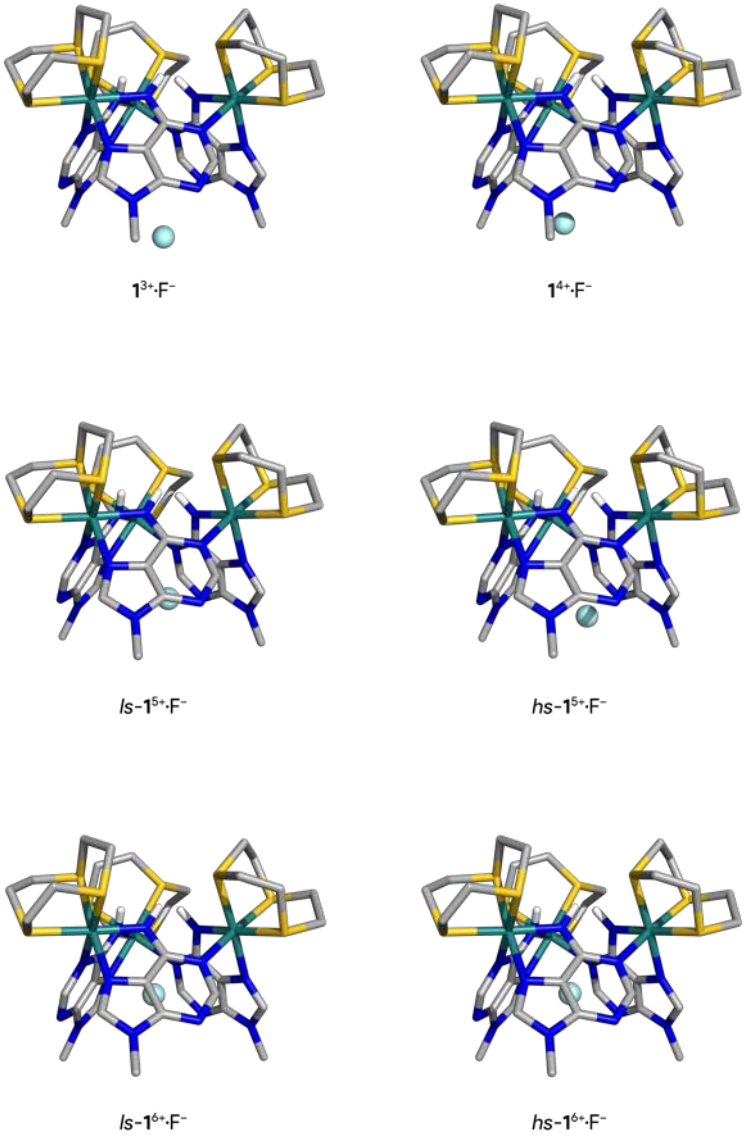

Fig. S29. DFT optimised structures of the $\mathbf{1}^{n+}\cdot F^-$ associations, with the anion hosted in the β pocket. The hosts' C–H hydrogen atoms were hidden for clarity.

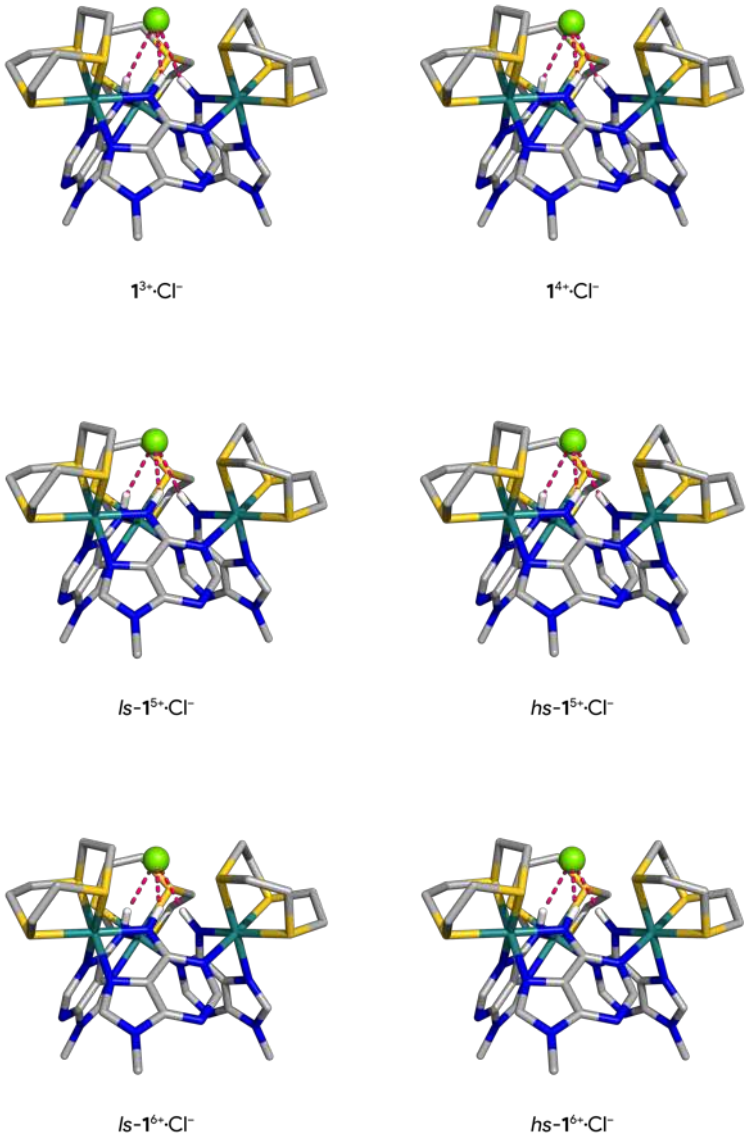

Fig. S30. DFT optimised structures of the $\mathbf{1}^{n+}\cdot Cl^-$ associations, with the anion hosted in the α pocket. The N–H···Cl^- hydrogen bonds are drawn as pink dashed lines. The hosts' C–H hydrogen atoms were hidden for clarity.

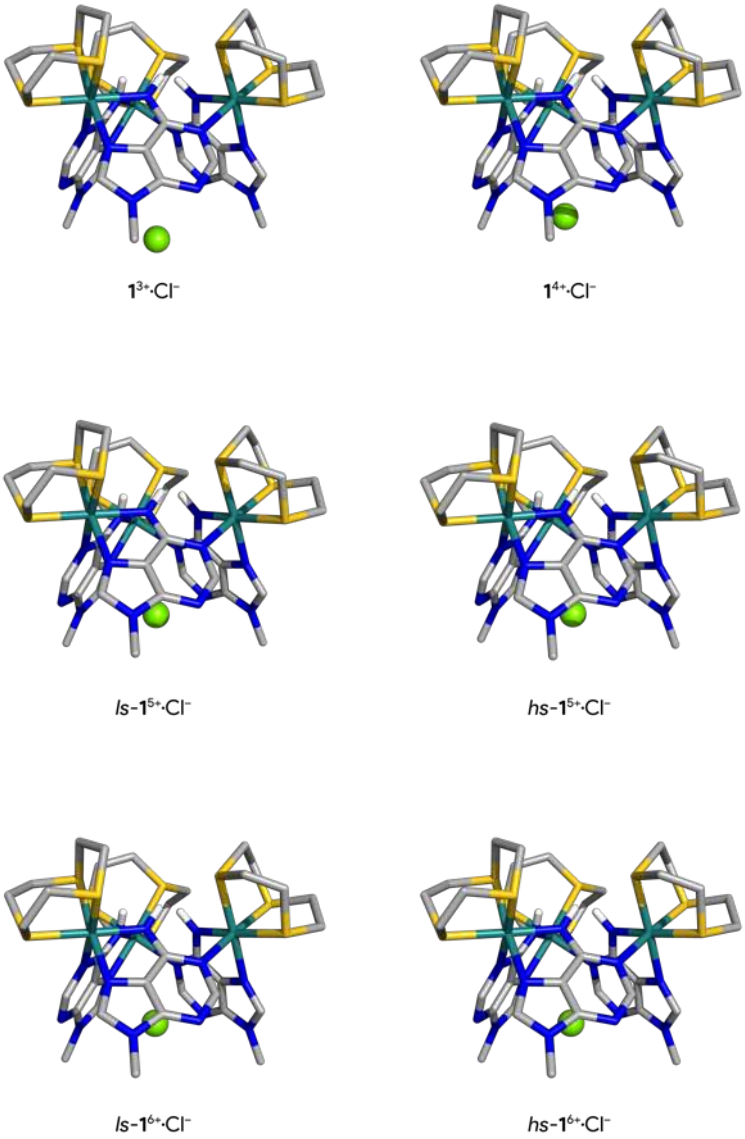

Fig. S31. DFT optimised structures of the $\mathbf{1}^{n+}\cdot Cl^-$ associations, with the anion hosted in the β pocket. The hosts' C–H hydrogen atoms were hidden for clarity.

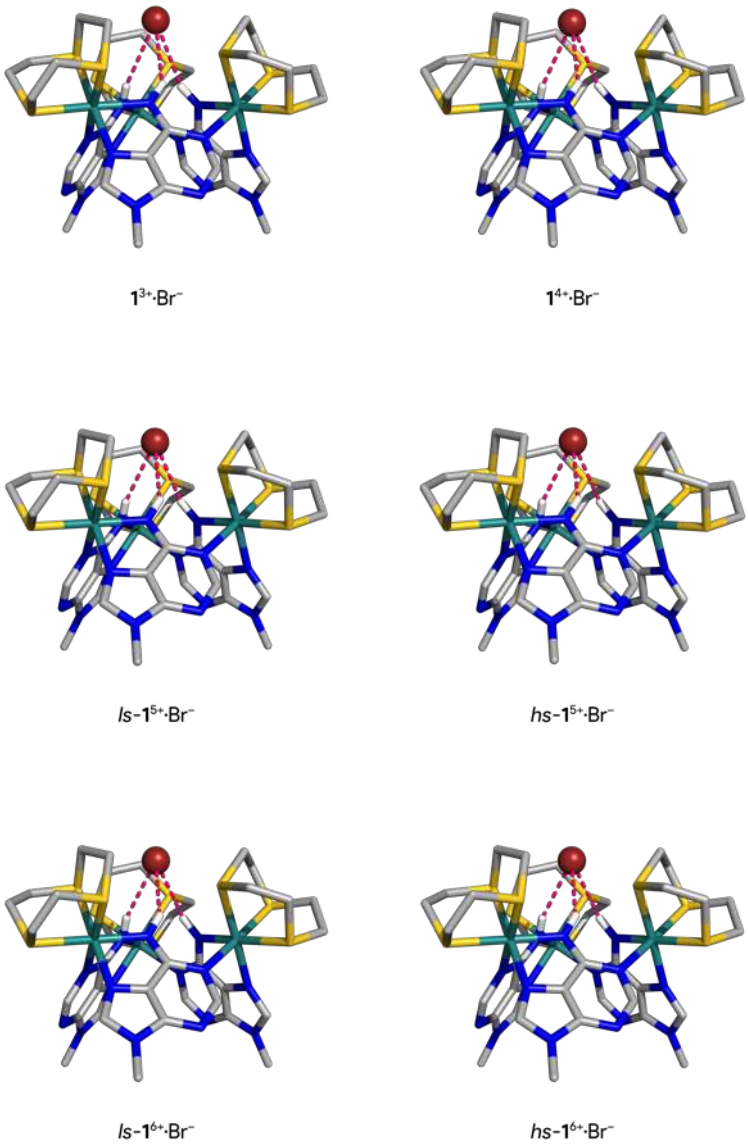

Fig. S32. DFT optimised structures of the $\mathbf{1}^{n+}\cdot Br^-$ associations, with the anion hosted in the α pocket. The N–H···Br⁻ hydrogen bonds are drawn as pink dashed lines. The hosts' C–H hydrogen atoms were hidden for clarity.

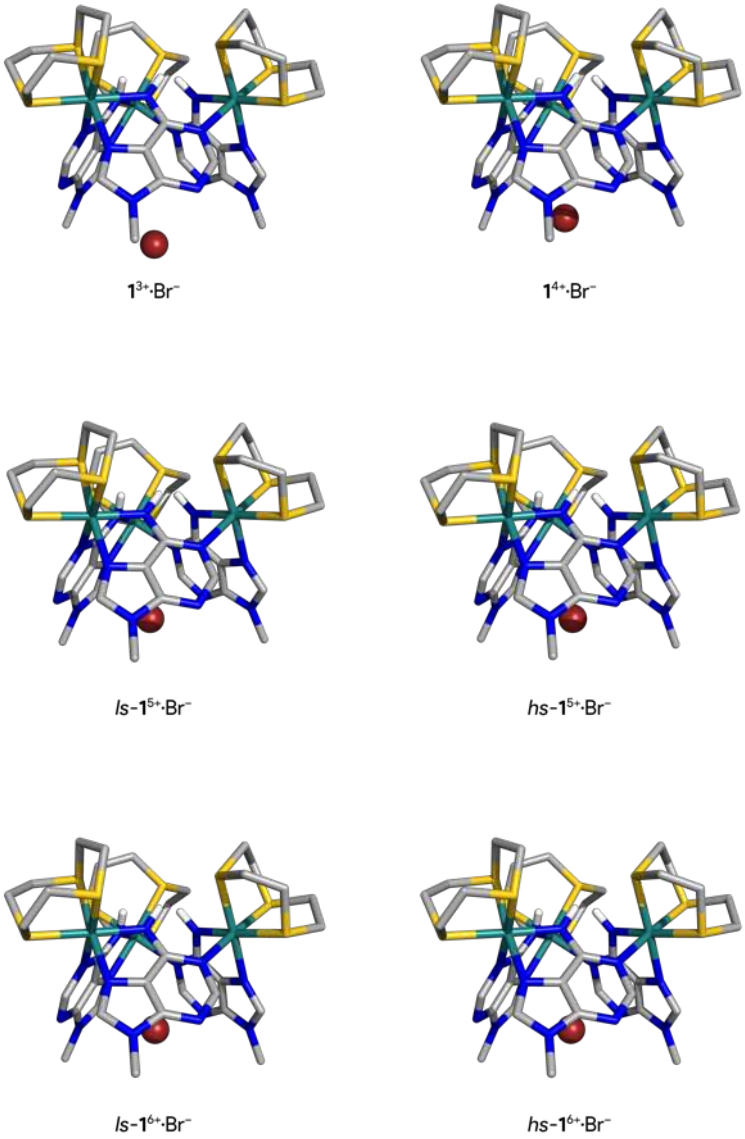

Fig. S33. DFT optimised structures of the $\mathbf{1}^{n+}$·Br⁻ associations, with the anion hosted in the β pocket. The hosts' C–H hydrogen atoms were hidden for clarity.

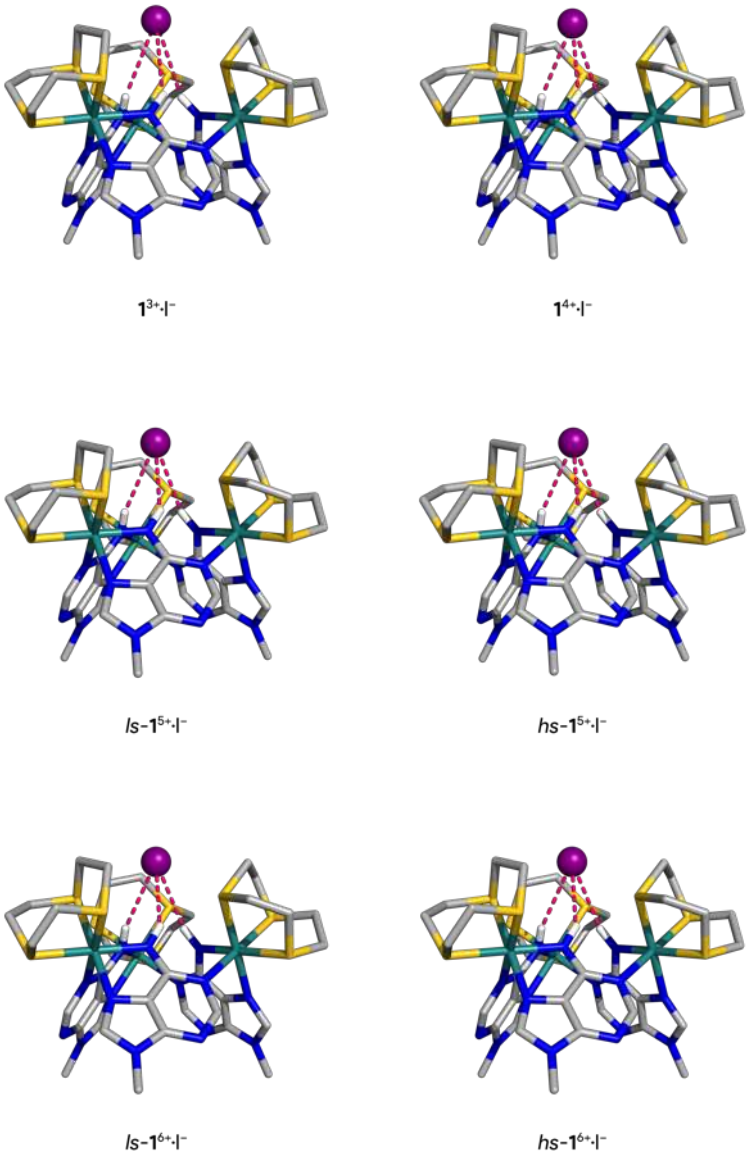

Fig. S34. DFT optimised structures of the $\mathbf{1}^{n+}\cdot\mathrm{I}^-$ associations, with the anion hosted in the α pocket. The N–H···I⁻ hydrogen bonds are drawn as pink dashed lines. The hosts' C–H hydrogen atoms were hidden for clarity.

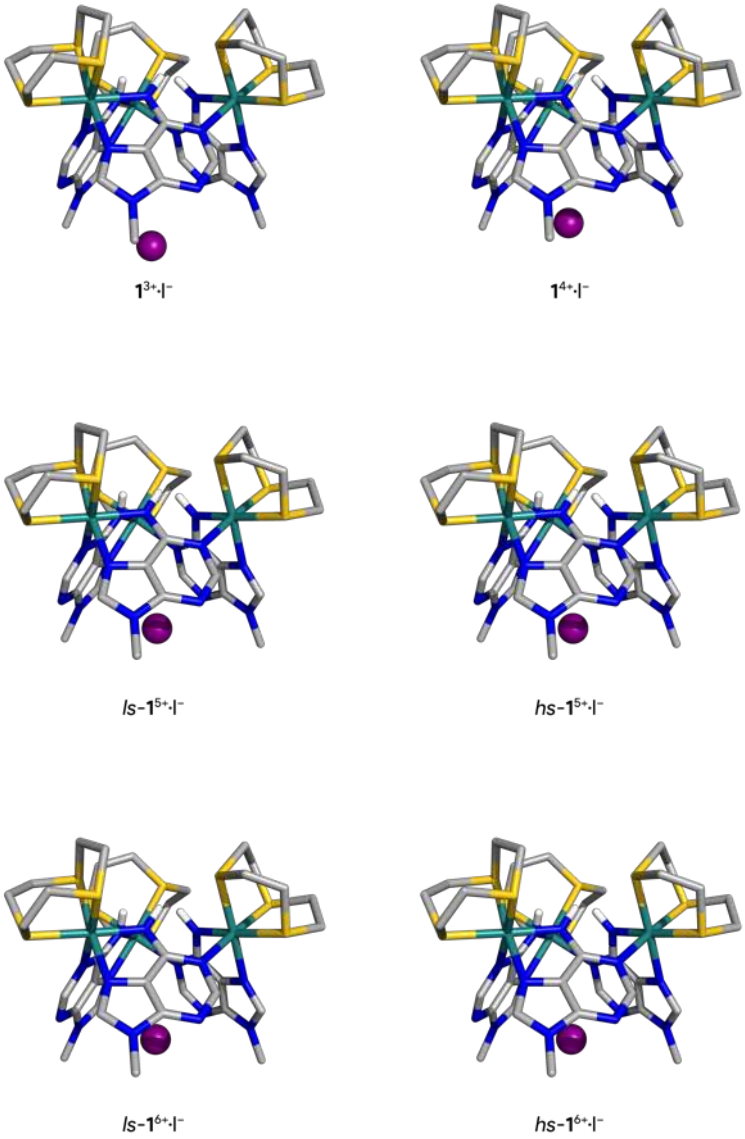

Fig. S35. DFT optimised structures of the $\mathbf{1}^{n+}\cdot\mathrm{I}^-$ associations, with the anion hosted in the β pocket. The hosts' C–H hydrogen atoms were hidden for clarity.

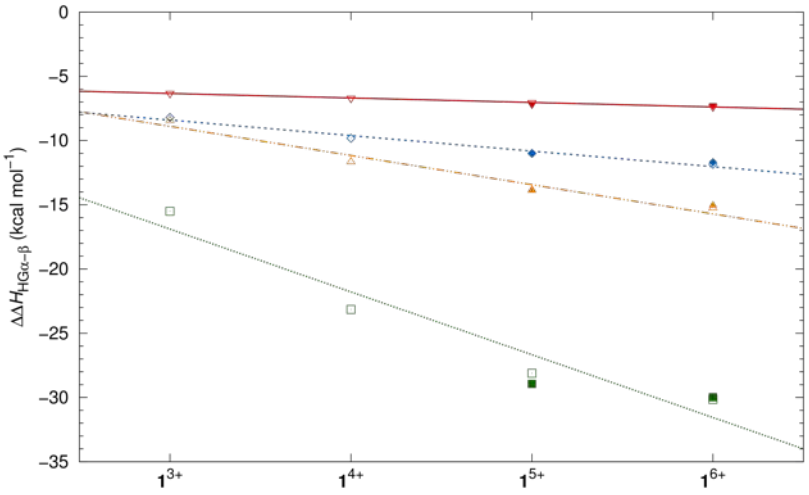

Fig. S36. Variation of $\Delta\Delta H_{HG\alpha-\beta}$ (kcal mol^{-1}) *vs.* $\mathbf{1}^{n+}$ oxidation state in the DFT optimised structures of the F^- (□), Cl^- (△), Br^- (◇) and I^- (▽) host-guest associations (all $R^2 \geq 0.938$). The high-spin electron configurations are represented by the filled points (■, ▲, ◆and ▼), but they might overlap with the low-spin points as the $\Delta\Delta H_{HG\alpha-\beta}$ energy is comparable between the two spin states.

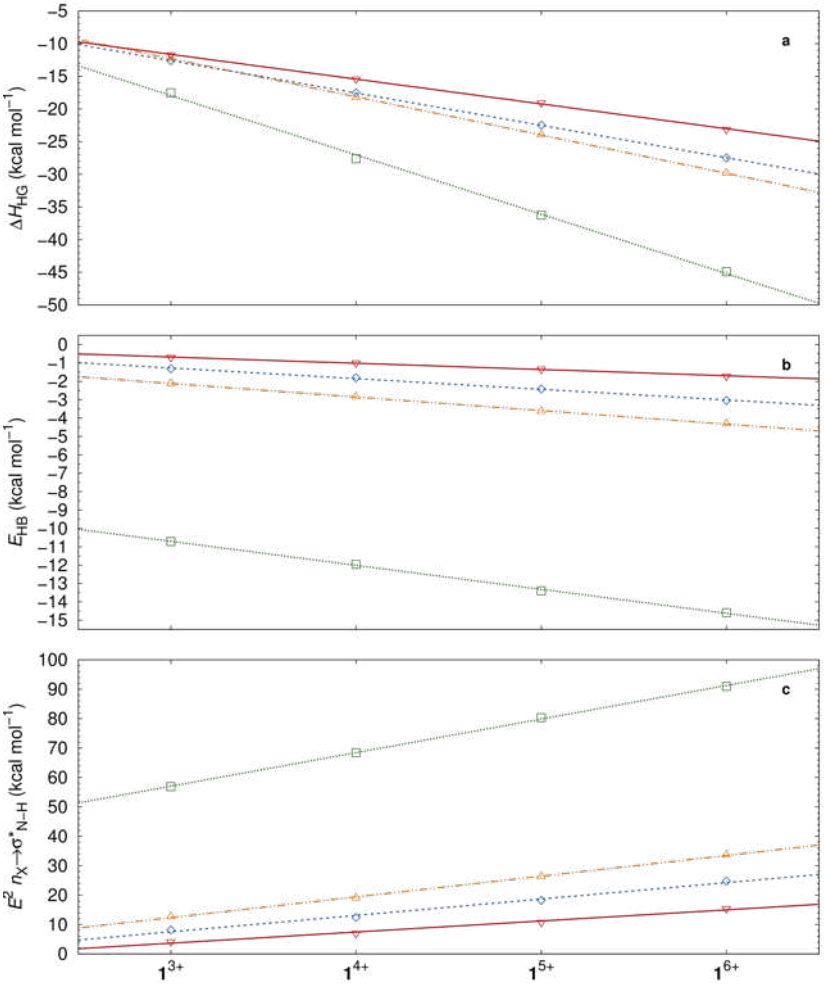

Fig. S37. Quantum parameters *vs.* $\mathbf{1}^{n+}$ oxidation state for the anion associations of $\mathbf{1}^{n+}$ and F^- (□), Cl^- (△), Br^- (◇) and I^- (▽), together with the corresponding linear fits: **a** Variation of the ΔH_{HG} (kcal mol^{-1}) between $\mathbf{1}^{n+}$ and the halides ($R^2 \geq 0.998$); **b** Average E_{HB} energy values (kcal mol^{-1}) for the hydrogen bonds between $\mathbf{1}^{n+}$ and the halides ($R^2 \geq 0.996$); **c** Variation of the E^2 stabilisation energies of $n_X \rightarrow \sigma^*_{N-H}$ (kcal mol^{-1}, X = F^-, Cl^-, Br^- or I^-) for the N–H···X interactions ($R^2 \geq 0.988$). The points for the high-spin electron configurations are not represented as they would overlap with the low-spin configurations data.

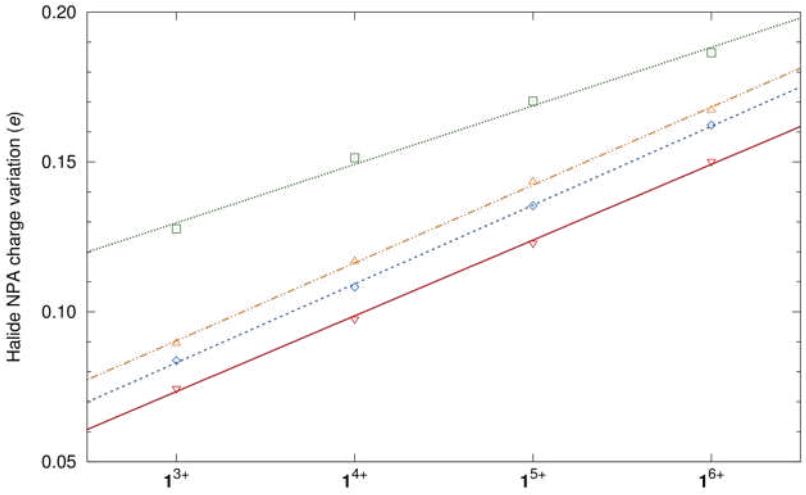

Fig. S38. Change in halide net charge (*e*) when hydrogen bonded to $\mathbf{1}^{n+}$in the DFT optimised structures, together with the corresponding linear fits ($R^2 \geq 0.993$). Key: F^- (□), Cl^- (△), Br^- (◇) and I^- (▽). The points for the high-spin electron configurations are not represented as they would overlap with the low-spin configurations data.

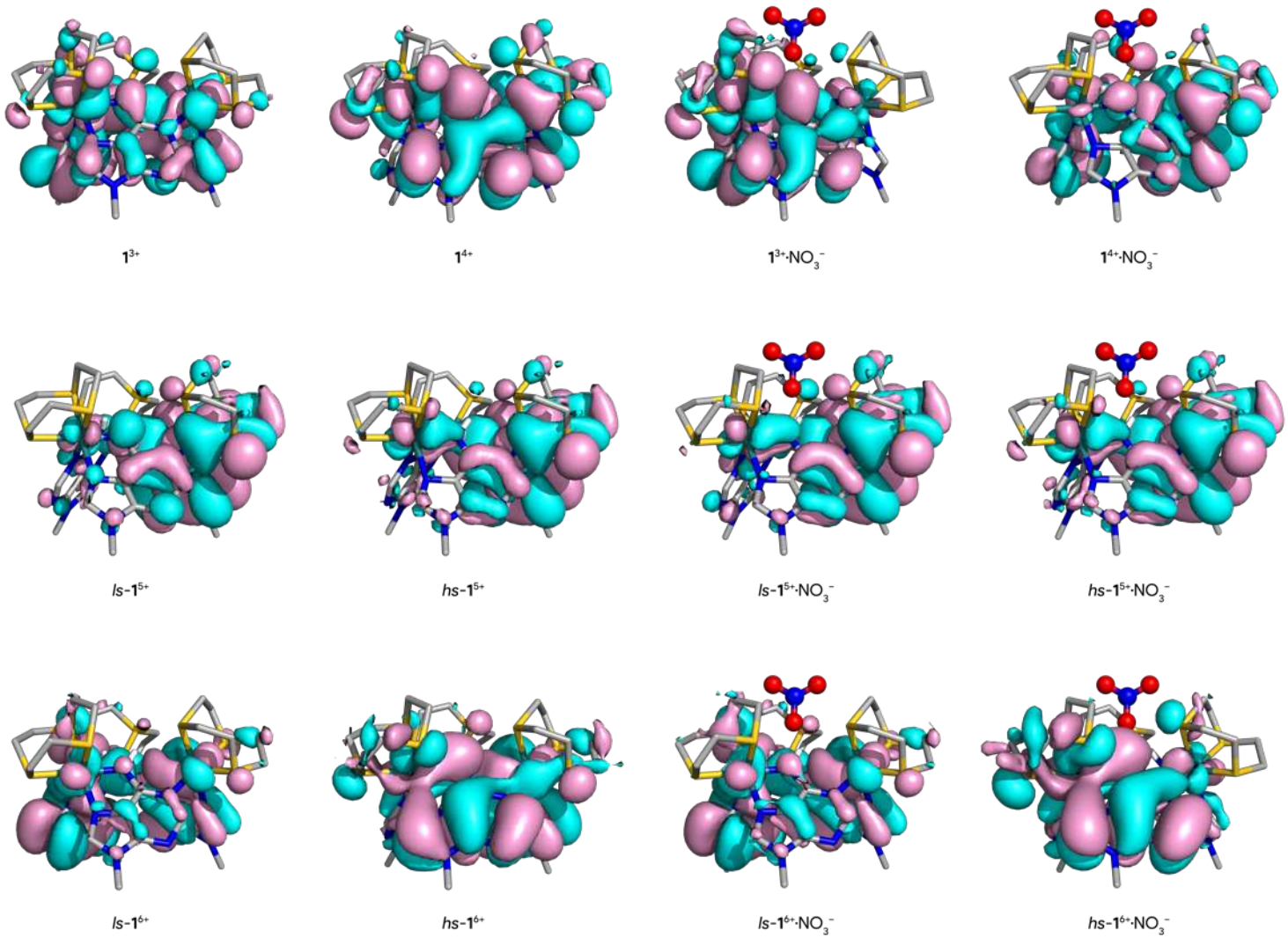

Fig. S39. HOMO surface plots (contour value 0.01 ea_0^{-3}) of $\mathbf{1}^{n+}$ and their NO_3^- associations in the DFT optimised structures.

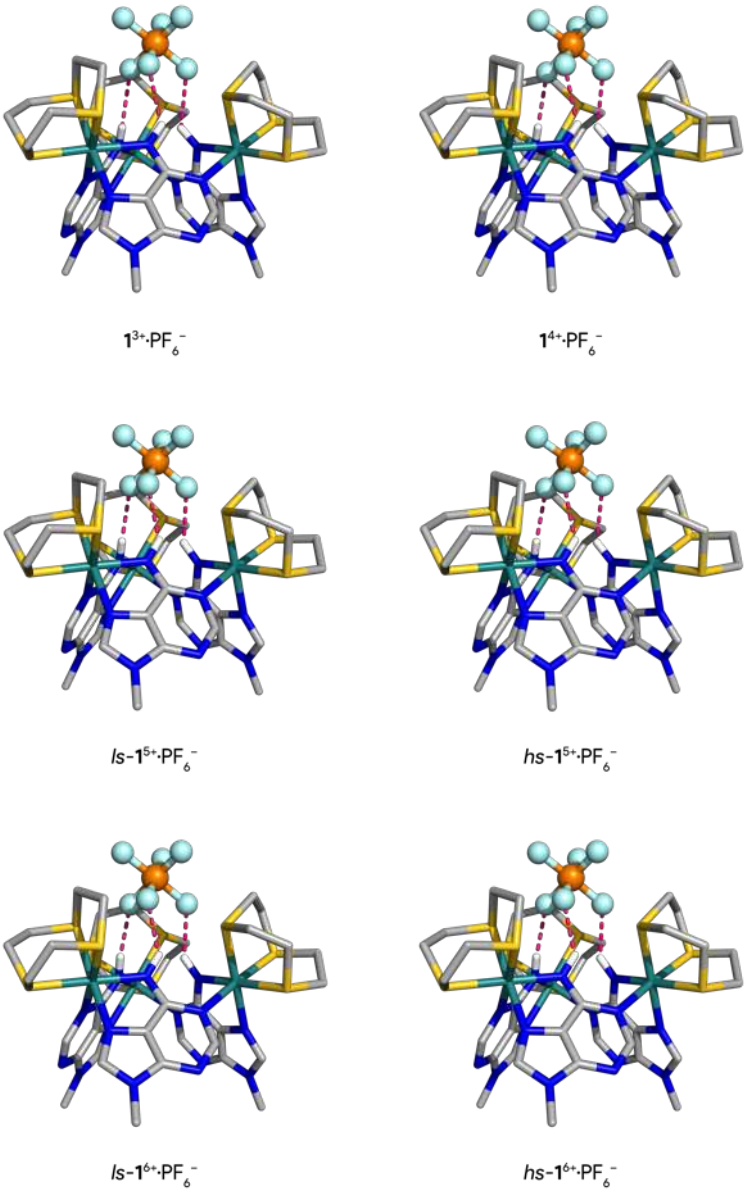

Fig. S40. DFT optimised structures of the $\mathbf{1}^{n+}\cdot PF_6^-$ associations, with the octahedral anion hosted in the α pocket. The N–H···F hydrogen bonds are drawn as pink dashed lines. The C–H hydrogen atoms were hidden for clarity.

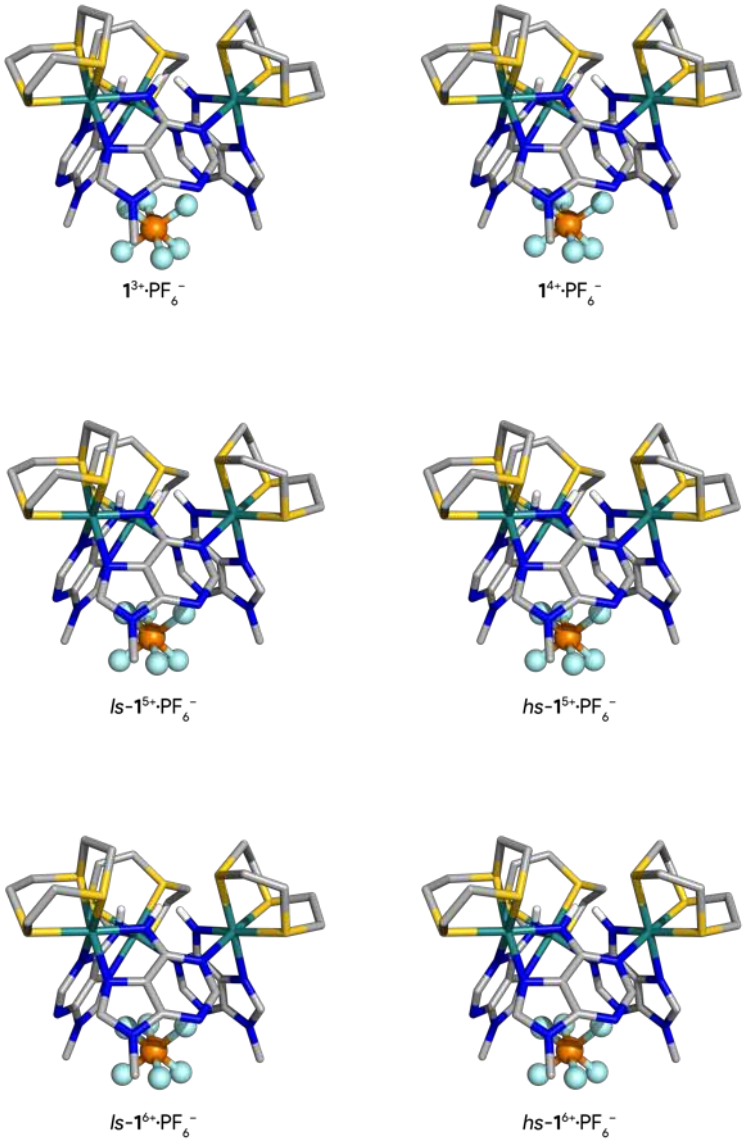

Fig. S41. DFT optimised structures of the $\mathbf{1}^{n+}\cdot PF_6^-$ associations, with the octahedral anion hosted in the β pocket. The hosts' C–H hydrogen atoms were hidden for clarity.

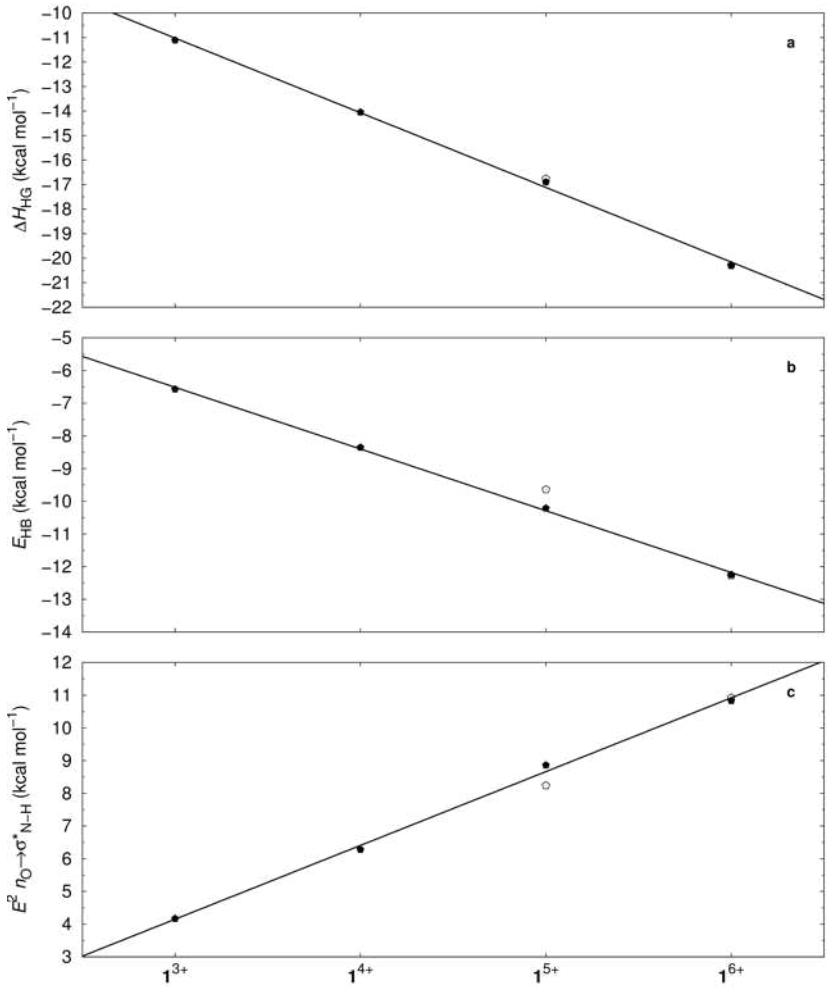

Fig. S42. Quantum descriptors assessed in the α pocket DFT optimised $\mathbf{1}^{n+}\cdot PF_6^-$ associations (⬟), together with their linear fittings: **a** Variation of the ΔH_{HG} (kcal mol^{-1}) between $\mathbf{1}^{n+}$ and PF_6^- (R^2 = 0.998); **b** Average E_{HB} energy values (kcal mol^{-1}) for the hydrogen bonds between $\mathbf{1}^{n+}$ and PF_6^- *vs.* $\mathbf{1}^{n+}$ oxidation state (R^2 = 0.999); **c** Variation of the E^2 stabilisation energies of $n_F \rightarrow \sigma^*_{N-H}$ (kcal mol^{-1}) for the N–H···F interactions (R^2 = 0.998). The high-spin electron configurations are represented by the open points (⬠), but they might overlap with the low-spin points as some given property is comparable between the two spin states.

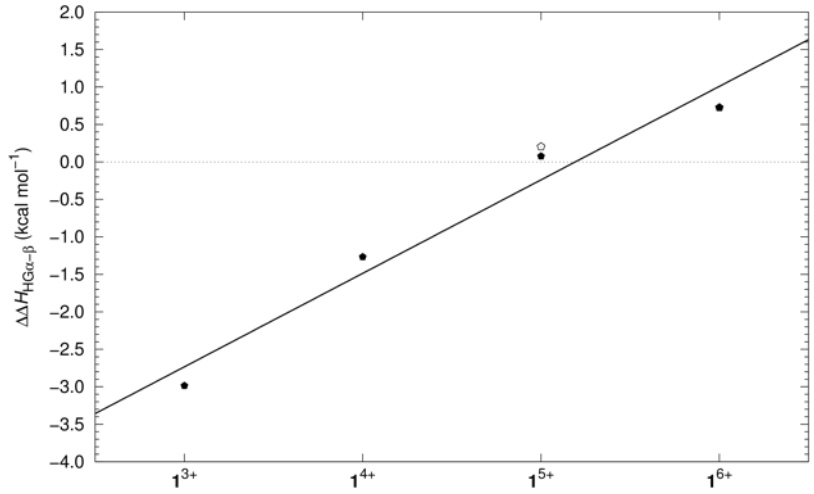

Fig. S43. Variation of $\Delta\Delta H_{HG\alpha-\beta}$ (⬟, kcal mol^{-1}) *vs.* $\mathbf{1}^{n+}$ oxidation state in the DFT optimised structures of the PF_6^- host-guest associations (R^2 = 0.964). The high-spin electron configurations are represented by the open points (⬠), but they might overlap with the low-spin points as the $\Delta\Delta H_{HG\alpha-\beta}$ energy is comparable between the two spin states.

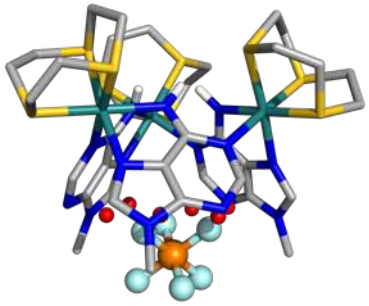

Fig. S44. Bond critical points (red spheres) of the π-anion interactions between the PF_6^- anionic guest and the $\mathbf{1}^{3+}$ host. The hosts' C–H hydrogen atoms were hidden for clarity.

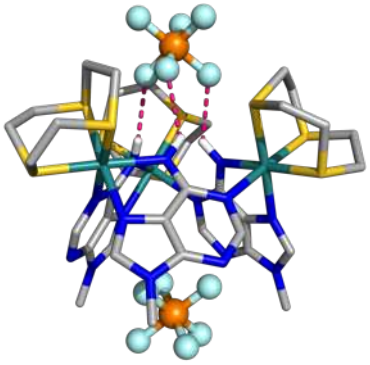

Fig. S45. DFT optimised structure of the $\mathbf{1}^{3+}\cdot(PF_6^-)_2$ association, with the octahedral anions hosted in the α and β pocket. The N–H···F hydrogen bonds are drawn as pink dashed lines. The C–H hydrogen atoms were hidden for clarity.

References

[1] Frisch, M. J.; Trucks, G. W.; Schlegel, H. B.; Scuseria, G. E.; Robb, M. A.; Cheeseman, J. R.; Scalmani, G.; Barone, V.; Mennucci, B.; Petersson, G. A.; Nakatsuji, H.; Caricato, M.; Li, X.; Hratchian, H. P.; Izmaylov, A. F.; Bloino, J.; Zheng, G.; Sonnenberg, J. L.; Hada, M.; Ehara, M.; Toyota, K.; Fukuda, R.; Hasegawa, J.; Ishida, M.; Nakajima, T.; Honda, Y.; Kitao, O.; Nakai, H.; Vreven, T.; J. A. Montgomery, J.; Peralta, J. E.; Ogliaro, F.; Bearpark, M.; Heyd, J. J.; Brothers, E.; Kudin, K. N.; Staroverov, V. N.; Keith, T.; Kobayashi, R.; Normand, J.; Raghavachari, K.; Rendell, A.; Burant, J. C.; Iyengar, S. S.; Tomasi, J.; Cossi, M.; Rega, N.; Millam, J. M.; Klene, M.; Knox, J. E.; Cross, J. B.; Bakken, V.; Adamo, C.; Jaramillo, J.; Gomperts, R.; Stratmann, R. E.; Yazyev, O.; Austin, A. J.; Cammi, R.; Pomelli, C.; Ochterski, J. W.; Martin, R. L.; Morokuma, K.; Zakrzewski, V. G.; Voth, G. A.; Salvador, P.; Dannenberg, J. J.; Dapprich, S.; Daniels, A. D.; Farkas, O.; Foresman, J. B.; Ortiz, J. V.; Cioslowski, J.; Fox, D. J. *Gaussian 09*, Revision D.01; Gaussian, Inc.: Pittsburgh PA, 2013.

[2] T. Yanai, D. P. Tew, N. C. Handy, *Chem. Phys. Lett.* 2004, *393*, 51-57.

[3] S. Grimme, J. Antony, S. Ehrlich, H. Krieg, *J. Chem. Phys.* 2010, *132*, 154104.

[4] B. Mennucci, J. Tomasi, R. Cammi, J. R. Cheeseman, M. J. Frisch, F. J. Devlin, S. Gabriel, P. J. Stephens, *J. Phys. Chem. A* 2002, *106*, 6102-6113.

[5] L. E. Roy, P. J. Hay, R. L. Martin, *J. Chem. Theory Comput.* 2008, *4*, 1029-1031.

[6] (a) T. Lu, F. Chen, *J. Comput. Chem.* 2012, *33*, 580-592; (b) T. Lu, F. Chen, *J. Mol. Graph. Model.* 2012, *38*, 314-323.

[7] R. F. W. Bader, *Atoms in Molecules: A Quantum Theory*, Oxford University Press, 1991.

[8] F. Weinhold, C. R. Landis, *Chem. Educ. Res. Pract.* 2001, *2*, 91-104.

[9] E. D. Glendening, C. R. Landis, F. Weinhold, *J. Comput. Chem.* 2013, *34*, 1429-1437.

[10] C. P. Kelly, C. J. Cramer, D. G. Truhlar, *J Phys Chem B* 2007, *111*, 408-422.